

Thermal imaging as a method to study the effect of induced ischemia on vasomotion activity

ANNABEL BANTLE, CHRISTIAN KORFITZ MORTENSEN, TOBY STEVEN WATERSTONE

December 12, 2017

Abstract

Vasomotion is an auto-regulation mechanism that optimizes blood distribution within the microcirculatory system. Thermal imaging is an interesting approach to measure this phenomena. Previous studies have detected that vasomotoric blood flow is quantifiable as temperature micro oscillations in the frequency range of 0,005 - 0,15 Hz. Four healthy subject was recruited to investigate the possibilities of measuring changes in vasomotoric blood flow caused by partial occlusion of blood supply by using thermal imaging. The temperature oscillations in the skin were measured with an infrared camera. Measurement were done under normal conditions and with 50% restriction of hands blood supply by brachial cuff. Data processing involved correction of artifacts seen in the temperature recording. An investigation seeking reasons for these artifacts led to findings of limitations in the thermal camera used for recording. Morlet continuous wavelet transform was used on the corrected temperature recording to find the frequency content in the micro temperature oscillations. Statistical analysis of the mean amplitude values within the frequency bands showed no significant difference between the magnitudes of uncuffed and cuffed. Results show thermal imaging might not be sensitive enough to detect vasomotion and clear limitations in the experimental setup.

I. INTRODUCTION

Vasomotion is the phenomena of oscillating changes in the capillary vessel diameter enforced by smooth muscle cells. This phenomena occurs in the microcirculatory system as an autoregulatory mechanism that optimizes blood distribution within the microcirculatory system.[1-4] Although there have been several studies, which have dealt with the occurrences of vasomotion within the capillary network, this area is not completely investigated.[5,6,7] However with a better knowledge of vasomotion it might be possible to add new parameters in the monitoring of intensive care patients. Particularly patients in danger of developing hypoxia due to shock as this affects alterations in the microcirculatory system and interferes with the perfusion.[8,9] New methods for studying vasomotoric activity arise and thermal

imaging presents advantages in larger sample area and by being non invasive. Previous studies detected that the vasomotoric blood flow is quantifiable as temperature micro oscillations within three frequency bands of endothelial (0,005 – 0,02Hz), neurogenic (0,02 – 0,05Hz) and myogenic (0,05 – 0,15Hz) origin. [1,5,6,10] Therefore the interest of this study is to investigate thermal imaging's ability to detect, if there are vasomotoric changes in the micro temperature oscillations of skin depending on hypoxia in the observed area.

II. METHODOLOGY

i. Subjects

Four healthy subjects (3 males and 1 female, average age 30.5 years) were recruited. Subjects were recruited within the project group.

Two subjects were right handed and two left handed. No subjects consumed caffeine, alcoholic beverages, or medicine before the experiment. All subjects were aware of experiment procedure and were willing to participate. Subjects showed no signs of cardiac disease or tremors.

ii. Test setting

Subjects were placed in an upholstered adjustable chair for a comfortable sitting position. The hand was stabilized by a vacuum pillow covered with microfiber tissue, which was attached on the armrest. Xenics Gobi 640 17m GigE infrared camera (Xenics NV, Belgium) was positioned with a tripod 37,5 ± 1,0 cm over subjects dominant hand and connected via Ethernet cable with a computer. The setup is shown in figure 1.



Figure 1: Test setting at Region Hospital Nordjylland showing setup of chair, thermal camera and computer.

iii. Software setting

Xeneth 2.6 software (Xenics NV, Belgium) installed on computer was used for data acquisition. The sampling rate was set to 6,25 Hz, the file format to a raw data .xvi file and both, room and ambient temperature, to 25°C and emissivity of observed object to 1.

iv. Experimental procedure

The experiment involved 2 x 20 min data acquisition periods. One under normal conditions

without the presence of hypoxia in the targeted hand, and another where blood flow restriction enforces hypoxia. The camera was set to warm up for at least 15 min. Subjects. Meanwhile systolic blood pressure was measured to determine total occlusion pressure (TOP) of subjects dominant arm. Needed cuff pressure (p_{cuff}) for restricting 50% blood flow was calculated with $p_{cuff} = TOP \times 0.3$.[11] The subjects had at least 30 minutes to adjust to the room temperature.

The cuff for enforcing blood flow restriction in the second acquisition period was affixed on subjects dominant arm without tightening it. Subject is placed in the chair and its dominant hand is stabled with the vacuum pillow. Lens focus was adjusted for a sharp image of the hand.

After the first measurement under normal conditions, pressure in the cuff was set to enforce 50 % blood flow restriction. The subject did not move the hand while cuff tightening. To minimize any possible movement bias the subject was not allowed to move or speak during the whole procedure.

v. Data processing

v.1 Preparation of data

The acquired xvi. files were read and processed in MATLAB R2017b. The header in the beginning of each file and frame was removed. Afterwards the raw uint 16 pixel intensities was divided into frames.

v.2 Regions of interest

Regions of interest (ROIs) were selected on behalf of getting full representation of the hand. As shown in figure 2 originating from the fingertips elongating down the hand to the beginning of the wrist. 28 ROIs were chosen. Each region represent one pixel intensity in the 480 x 640 image matrix.

This pixel represents an area of the hand with a diameter of 417 μm .

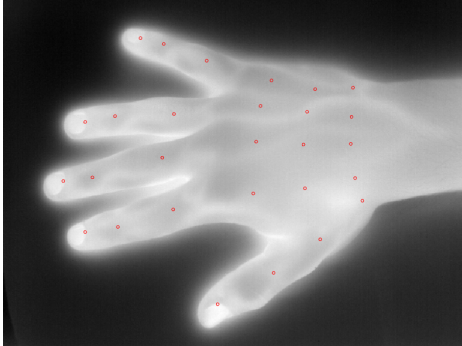


Figure 2: Frame from thermal image of subject 1. Red dots showing the 28 ROIs.

v.3 Artifacts

Under visual inspection of the temperature trace over time, some unexplainable jumps were present. These jumps were characterized as artifacts made by the camera. From the raw data of all regions four types of artifacts were characterized. A noise component is observed during the whole recording. Adjustments of the shutter from non-uniformity correction due to the internal temperature. The intervals between two jumps contain a drift component. An overall drift component can also be observed. Figure 4 shows the signal of one ROI to present the occurring artifacts.

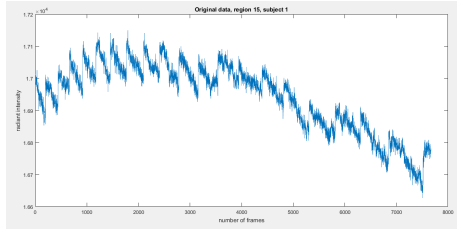


Figure 3: The original data of region 15 in the uncuffed recording of subject 1 used as an example to outline the artifacts. The intensity is shown over time.

v.4 Correction method

The shutter adjustments and the drift between these adjustments seen in figure 4 corrupted the original the most. Therefore a correction

method based on linear regression was implemented. A linear regression is made on each drift between shutter adjustments. The found regression lines are put together at the middle point of an adjustment forming a new temperature recording base. The residuals are then projected on to the newly corrected base forming a new temperature trace.

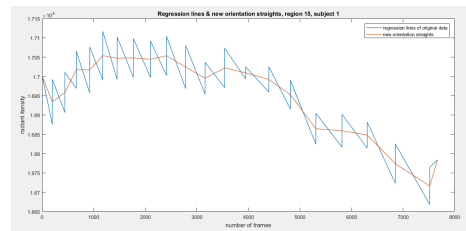


Figure 4: Connected regression line of the original data of region 15 in the uncuffed recording of subject 1 in blue. New created orientation line of the same recording in the same region shown in red.

v.5 Continuous wavelet transformation

Analysis of the corrected data is done in time frequency domain by the use of the Morlet continuous wavelet transform (CWT). The CWT present higher resolution of frequency content in low frequency signals, compared the usually used frequency analysis method of Fourier transforms.[5,6] A scalogram showing the time-frequency analysis content of the signal given as output of the CWT can be seen in figure 5.

The jumps within the signal are shown as high bright spikes in the scalogram. In figure 5 those spikes are marked with red arrows.

The signals of some ROIs contain still jumps after application of the correction method. Therefore each signal and its scalogram has been submitted a visual control. Five ROI which showed in all measurements good response to the correction method were selected for further data processing. All five ROI are located in the back of the hand.

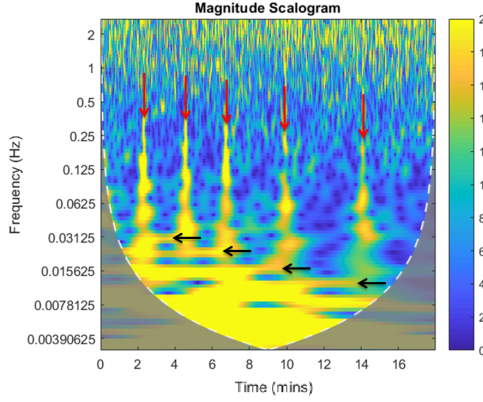


Figure 5: Scalogram showing the time-frequency content of subject 3's uncuffed recording in ROI 8.

vi. Statistical approach

To test the statistical significance of the difference between both condition a paired t-test with a significance level of $\alpha = 0.005$ is applied regarding the null-hypothesis $h_0 = \text{"there is a difference in both conditions"}$. Therefore the outcome data of each subject's scalograms are all frequency bands considered down to the total mean magnitude.

III. RESULTS

The box-plots shown in figure display the mean magnitude for each subject ordered by color in both conditions. The line connecting uncuffed and cuffed condition indicates if magnitude increased or decreased. With the values visualized by the box-plots in figure a paired t-test provides the following p-values (table 1). These

	P-endo	P-myo	P-neuro
ROI 10	0.7116	0.8454	0.9389
ROI 14	0.6254	0.9237	0.6955
ROI 20	0.4141	0.9237	0.8004
ROI 21	0.4062	0.9564	0.8452
ROI 22	0.3826	0.9323	0.1552

Table 1: Table showing the p-values corresponding to specific ROI in correlation with frequency band.

p-values result in rejecting the null-hypothesis $h_0 = \text{"there is a difference in both conditions"}$.

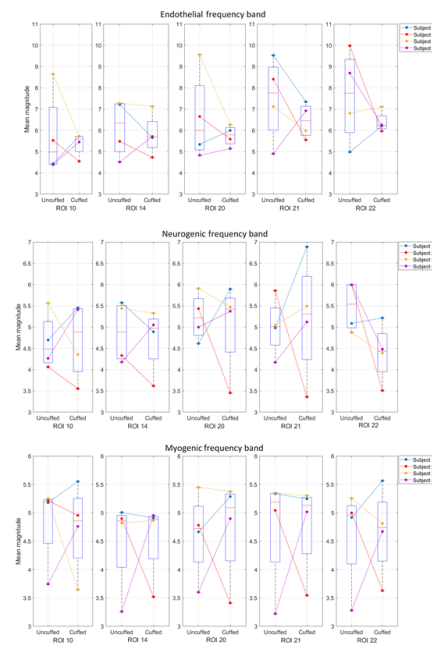


Figure 6: Box-plot showing the mean magnitudes for each subject within endothelial, neurogenic and myogenic frequency bands.

IV. DISCUSSION

This study investigates the thesis, if thermal imaging is sensitive enough to measure the effects of vasomotion activity, and thereby investigate if changes in the microcirculatory system caused by a 50 % restriction of blood flow occur.

i. Results

The obvious assumption, based on the presented p-values, that there are no changes in the microcirculatory system or rather in vasomotion by 50% restriction of blood flow can be substantiated by two reasons. Firstly independence of the microcirculatory system in terms of vasomotion activity. The available amount of blood in the microcirculatory system is dependent on the amount of blood the macrocirculatory system provides which means that the microcirculatory system is not independent. Consequently this explanation can be excluded. Another explanation for the insignificant result

could be by incorrect brachial occlusion. Incorrect occlusion would yield insufficient restriction for affecting the microcirculatory system. A wrong occlusion pressure could be the cause of this. The blood pressure measurements of three subjects delivered high values around 140 mmHg and 150 mmHg. Since those three subject were in different age and shape, a suspicion for incorrect values arise. Even if the blood pressure monitor delivered wrongly high values, the outcome of the second measurement would not have been influenced negatively. This would only lead to a calculated occlusion pressure higher than the one needed to reach the intended restriction, which would just lead to a larger difference between both conditions. It would be more problematic with a occlusion level to low. All blood pressure measurements were conducted and verified by a professional anesthesiologist.

ii. Critique of study design

The small sample size of four subjects applied to the statistical methods are not sufficiently meaningful. With a larger amount of subjects this study would get a more meaningful result. A larger amount of subjects might therefore have provided a significant difference between both conditions. An even gender distribution might also have been preferable.

Other limitations might be that the subjects hands had to be stabilized by a vacuum pillow with the assumption the subjects were still, but this does not give sufficient support to inhibit every movements of the subject. A mechanism for better stabilization of the hands should be included. An approach to compensate for instability of the hand during the experiment could have been to include image alignment in the data processing to limit the drawbacks of possible movements in the recordings. Furthermore with the used setup exact same conditions for each subject cannot be granted. For instance the room temperature should have been measured beforehand and taken into consideration before the start of each experiment to create the same conditions for all subjects. The presetting

of the room temperature might have affected the data. This suspicion is enhanced by regarding subject 1's hand temperature which was 38°C. Also by regarding the hand temperature of 26°C of subjects 2 and 3, who had cold hands during the measurement, this suspicion is enhanced. The software settings should be verified and if necessary changed beforehand of the experiment. An optimization of the test setting would require a more controlled setup of the experiment and a thermal camera of higher quality preferable of a cooled type.

iii. Limitations in using thermal camera

Due to the corrupted temperature reading the correction method was implemented, which clearly affects parts of the signal in specific ROIs. The pixel drift increases with increasing distance to the center of the thermal image why pixel drift of ROIs located in the outer areas of the thermal image cannot be completely compensated for with the implemented correction method. The explanation for this is likely that the correction method is based on the assumption that the drift component in every interval is linear. This assumption might be wrong and a correction method that uses another regression method or combines different regression methods might adjust the artifacts in a better way. As a result the ROIs located in the outer area of the thermal image were excluded from the data analysis. Another camera might also be preferable to reduce the risks of technical artifacts like these.

Furthermore the smaller the observed area the closer the thermal camera has to be to this area. Thus the area represented by one pixel gets smaller. Within this study one pixel represents an area with a diameter around 417μm. Whereas previous studies observed smaller areas which means that the pixel represent a smaller area. With the use of a larger ROI, it might be that the amount of inverse dilating capillaries is equal and thereby canceling each other out. Due to inverse dilating capillaries there might be no changes over time

measurable because the frequency contents are occurring alternating in the different capillaries. In addition, it is obvious that the artifacts content in the signal is significantly higher than in the temperature signals detected in previous studies. Comparing the signals the question arises if the artifacts overlaps or suppresses the frequency content of vasomotoric activity. Even though temperature changes over time in the skin were detected, it is uncertain, if this signal just represents the general skin temperature or also vasomotoric activity.

V. CONCLUSION

The results of this study indicate that thermal imaging is not sensitive enough for detecting vasomotion activity. There have been no findings of a statistical significant difference in the dataset between the two conditions investigated, indicated by the high p-values in table 1. Despite no findings, this study provides information about key points that should be considered when with thermal imaging, for instance that the regions that is of most interest should be placed in the center of the thermal image. Further investigation in this field is needed, to show thermal imaging as a promising technique for detecting vasomotion activity.

VI. ACKNOWLEDGMENT

The authors would like to thank Lasse Riis Østergaard, Carsten Dahl Mørch and Andrei Citubaturiu for the cooperation and great advice during this study. Furthermore we are Region Hospital Nordjylland thankful for the use of their facilities during the experiment.

REFERENCES

- [1] Tang YL, He Y, Shao HW, Mizeva I. Skin temperature oscillation model for assessing vasomotion of microcirculation. *Acta Mechanica Sinica*. 2015; 31(1): 132-138.
- [2] Bartholomwe EF Martini FH, Nath JL. Fundamentals of Anatomy and Physiology Ninth Edition. Pearson, 2012, p. 1272. isbn: 13: 978-0-321-70933-2.
- [3] H. Nilsson. Vasomotion: Mechanisms and Physiological Importance. In: Molecular Interventions 3.2 (2003), pp. 79-89. issn: 1534-0384. doi: 10.1124/mi.3.2.79. url: <http://molinterv.aspetjournals.org/cgi/doi/10.1124/mi.3.2.79>.
- [4] Steven S. Segal. Regulation of blood flow in the microcirculation. In: Microcirculation 12.1 (2005), pp. 33-45. issn: 10739688. doi: 10.1080/10739680590895028.
- [5] Mary Jo Geyer et al. Using wavelet analysis to characterize the thermoregulatory mechanisms of sacral skin blood flow. In: Journal of rehabilitation research and development 41.6A (2004), pp. 797-806. issn: 0748-7711. doi: 10.1682/JRRD.2003.10.0159.
- [6] Sagaidachnyi et al. Determination of the amplitude and phase relationships between oscillations in skin temperature and photoplethysmography-measured blood flow in fingertips. In: Physiological measurement 35.2 (2014), pp. 153-66. issn:1361-6579. doi: 10.1088/0967-3334/35/2/153. url:<http://www.ncbi.nlm.nih.gov/pubmed/24399251>.
- [7] Wei Min Liu et al. Reconstruction of thermographic signals to map perforator vessels in humans. In: Quantitative InfraRed Thermography Journal 9.2 (2012), pp. 123-133. issn: 21167176. doi: 10.1080/17686733.2012.737157.
- [8] Ronald V. Maier. Approach to the Patient with Shock. In: Harrison's

Principles of medicine 18 (2012). url:
<http://accessmedicine.mhmedical.com/content.aspx?bookid=331%7B%5C&%7Dsectionid=40727056>.

- [9] Can Ince. The microcirculation is the motor of sepsis. In: Critical care (London, England) 9 Suppl 4.Suppl 4 (2005), S13-9. issn: 1466-609X. doi: 10.1186/cc3753. url:<http://www.ncbi.nlm.nih.gov/pubmed/16168069%7B%5C%7D5Cn>
- [10] Sagaidachnyi et al. Thermography-based blood flow imaging in human skin of the hands and feet: a spectral filtering approach. In: Physiological Measurement 38.2 (2017), pp. 272-288. issn: 0967-3334. doi: 10.1088/1361-6579/aa4eaf. url:<http://www.ncbi.nlm.nih.gov/pubmed/28099162%7B%5C%7D5Cn><http://stacks>.
- [11] J. Grant Mouser et al. A tale of three cuffs: the hemodynamics of blood flow restriction. In: European Journal of Applied Physiology 117.7 (2017), pp. 1493-1499. issn: 14396319. doi: 10.1007/s00421-017-3644-7.

Thermal imaging as method to study effect of induced ischemia on vasomotion activity

7. Semester project - Fall 2017

Group 7407



AALBORG UNIVERSITET
STUDENTERRAPPORT

7th Semester, Project

School of Medicine and Health

Biomedical Engineering and Informatics

Fredrik Bajers Vej 7A

9220 Aalborg

Title:

Thermal imaging as method of studying vasomotion

Theme:

Don't know

Project period:

P7, Fall 2017

01/09/2017 - 20/12/2017

Projektgruppe:

17gr7407

Synopsis

Students:

Annabel Bantle

Christian Korfitz Mortensen

Toby Steven Waterstone

To be written

Supervisors:

Lasse Østergaard

Carsten Dahl Mørch

Andrei Ciubotariu

Pages: ??

Appendix: ??

Handed in: 20/12/2017

Abstract

also needs to be written

Preface

Needs to be written

- Tell about us as group, the place we study, something about the study
- Thank the supervisors

Contents

Part I	Background	1
1	Anatomy and Physiology	2
1.1	Macrocirculatory system	2
1.2	Microcirculatory system	3
2	Hemodynamics	6
2.1	Physiological Base	6
2.2	Physical Base	6
3	Vasomotion in disease	8
4	Methods of studying vasomotion	11
4.1	Thermal imaging	12
4.2	Laser Doppler flowmetry	12
4.3	Summarizing	13
5	Infrared Thermal Imaging	14
5.1	Introduction to thermal imaging	14
5.2	Measuring thermal energy	15
Part II	Methods	18
6	Study setup	19
6.1	Subjects	19
6.2	Test setting	20
6.3	Software setting	21
7	Interpretation of data	22
7.1	Continous wavelet transformation	22
Part III	Data analysis	25
8	Preparation of the data	26
8.1	Dividing the data into frames	26
8.2	Regions of interest	27
8.3	Artifacts in temperature recording	29
8.4	Correction method	29
9	Data processing	34

9.1	Scalogram interpretation	34
9.2	Selecting ROIs for statistical test	37
9.3	Statistical approach	37
Part IV	Results	38
10	Results	39
10.1	Wilcoxon signed rank test	39
Part V	Discussion	42
11	Discussion	43
A	Protocol	49
B	Evaluation table	53

Part I

Background

1 | Anatomy and Physiology

The following chapter outlines the functions of the cardiovascular system and focuses on its microcirculatory part. Further the phenomena of vasomotion is illustrated.

1.1 Macrocirculatory system

The main function of the cardiovascular system is the blood supply of the whole body and the transportation of metabolites. The propulsion of this is the heart. It generates the systolic blood pressure through the strength of left ventricle. The pressure difference between the heart and the periphery emerging from there, ensures the blood flow. The blood flows from regions with high pressure, like the aorta, to regions with low pressure, like the periphery.[1]

The heart supplies the body through the systemic and the pulmonary circuit with blood. Through these circuits the heart regulates the blood allocation with adjustment of stroke volume and heart frequency. The oxygen-rich blood accumulates in the left ventricle. From there the blood is pushed out through the aortic valve into the aorta and via the arteries spread into the whole body. The venous system returns the meanwhile low in oxygen blood back to the heart into the right atrium. From there the blood flows into the right ventricle and is pushed out through the pulmonary valve into the lung arteries. In the lungs gas exchange of the blood happens. Subsequent the oxygen-rich blood flows via the pulmonary veins back to the left heart to supply the body.[1]

As mentioned, there are two types of vessels, arteries and veins. The difference between those two types of vessels is that arteries transport the blood away from the heart and veins solely transport blood to the heart. There are also some differences in the structure of arteries and veins. Arteries consist of three different layers, tunica interna, tunica media and tunica externa. The tunica interna consists of vascular endothelium, the tunica media consists of smooth muscle cells and elastic fibres, the tunica externa consists of connective tissue and also elastic fibres. Furthermore, there are two different types of arterial vessels. In arteries of the elastic type prevail the elastic fibres in the tunica media. This allows an abrupt extension of the vessel during the systole and ensuing constriction, due to this the blood is transported. This phenomena is called windkessel function. In arteries of the muscular type prevail the muscular fibres in the tunica media. This allows regulation of the lumen by constriction and dilatation, whereby the resistance and the blood flow in the organs is regulated.[1]

Venous vessels are similarly structured like arterial vessels, however they are thinner and have also semilunar valves inside, to inhibit back flow inside the vessels. This system is supported by the skeletal muscles which help to hold up blood flow. The arterial and the venous vessel system are connected through the capillary system in the microcirculatory

system.[1]

1.2 Microcirculatory system

The heart and larger arteries and veins are associated with the cardiovascular system, but those are only used for transportation of blood. Instead it is the capillaries, that permeate most tissues, that is responsible for the perfusion of tissue. These are the only vessels which permit exchange between the vessel and the surrounding interstitial fluids. Factors that affect tissue perfusion is cardiac output, peripheral resistance and blood pressure. Capillaries are made not of single individual fluid conductors like veins and arteries, but instead formed into capillary beds. Here they work as a interconnected network of vessels. As mentioned before the arteries decrease in size the further they expand into the peripheral system. The small arteries divide into arterioles which further divide into dozen of capillaries. The capillaries merge into a venule after the blood has been de-oxygenated. A capillary is divided into two segments, first the metarteriole and second the capillary. The blood flow between arterioles and venules can also be a direct connection, made by an arteriovenous anastomosis. This works as a bypass diverting blood flow around the capillary bed. An example of the structure of the capillary bed can be seen on fig. 1.1.[1]

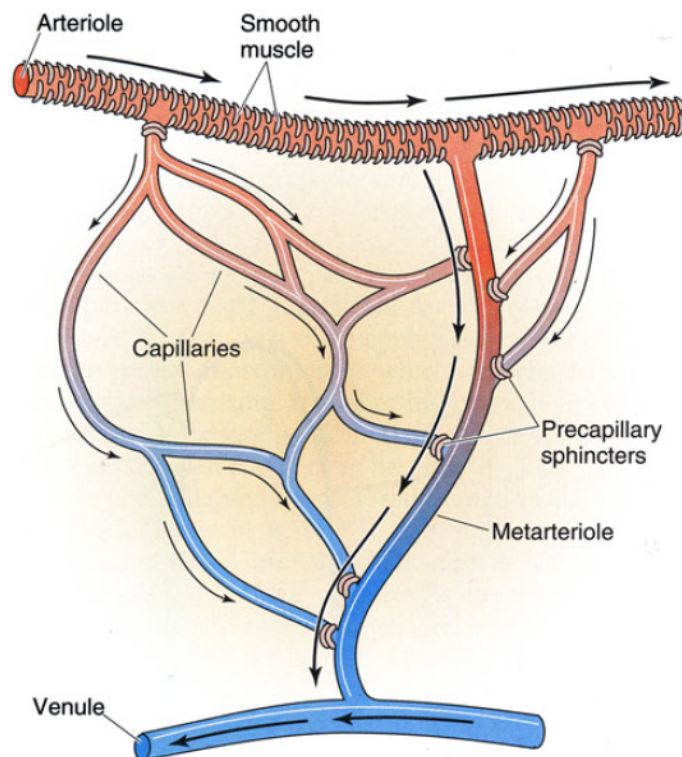


Figure 1.1: The basic structure of a capillary bed, with arteriole over the bed and a venule underneath.[1]

Each capillary entrance is controlled by a precapillary sphincter, which is composed of smooth muscle cells, that are able to contract or relax and thereby limit access of blood flow to certain capillaries. The blood flows relatively slow within the capillaries giving time for the two way exchange of nutrients and wastes. [1]

1.2.1 Vasomotion

The flow within the capillaries varies. This is among other thing due to the earlier mentioned precapillary sphincters opening and closing. The opening and closing of sphincters is part of the autoregulation process performed at a local level, to control the blood flow. The vascular system does not contain blood enough for every vessel a capillary beds to be filled with blood. Therefore only 25% of the vessels in a capillary bed contains blood, and vessels activity needs to be well coordinated. Thermoregulation and control of nutrition balance are the primary functions of the microcirculatory system. Local changes in concentration of chemicals and interstitial fluids eg. dissolved oxygen concentrations in tissue modulates the vascular smooth muscles activity. Constriction and dilation of the vessel is thereby regulated by this periodic activity, also known as vasomotion. [1, 2]

Under normal circumstances cardiac output remains stable and the control of local blood flow happens through local peripheral resistance within local tissues. The regulation of cardiovascular activity is controlled by local homeostatic mechanism. These make sure that demands such as oxygen and nutrients are meet and wastes are disposed.[1]

Physiological mechanism controlling vasomotion are not yet fully understood, but vascular smooth muscle activity has been shown to be roughly proportional to the tissue's metabolic demand for oxygen.[2] Studies also suggest that an increase in vasomotion activity enhances oxygen delivery[3]. Further have some factors that trigger homeostatic mechanism to alter the vasomotion been said to have an impact. Factors that trigger dilation is called vasodilators and can be some of the following:[1, 2]

- Decreased oxygen level or increased CO₂ level
- Lactic acid or other acids generated from tissue cells
- Nitric oxide NO released from endothelial cells
- Rising concentrations of potassium ions or hydrogen ions in the interstitial fluid
- Chemicals released during local inflammation
- Elevated local temperature

A vasodilation will result in increased oxygen, nutrients, buffers released to recreate homeostasis. Factors that stimulate constriction is called vasoconstrictors and can happen due to following:[1]

Chapter 1. Anatomy and Physiology

- Damaged tissue
- Aggregating platelets

Furthermore mechanisms regulation vasomotion can be divided into three origins. These are endothelial/metabolic, myogenic and neurogenic. Endothelial regulation is based on registered O₂, CO₂, lactate, and H⁺ levels and from this releases nitric oxide as a vasodilator. Myogenic regulation senses strain and stress in vessels, which cause the smooth muscle to depolarize, contracting the vessels. Otherwise when the ion channels in the muscles close, the blood vessels relaxes leading to vasodilation. Neurogenic signals is said to come from the sympathetic nervous system where these promote vasoconstriction.[4, 5, 6]

2 | Hemodynamics

Hemodynamics explains the movement or flow of blood. It is influenced by parameters like blood pressure, blood volume, cardiac output, blood composition, etc. It is possible to measure some of the hemodynamic parameters non-invasive, and also to calculate parameters.[1, 7]

2.1 Physiological Base

The regulation of the blood pressure happens with baroreceptors in the walls of the big arteries in chest and neck area. These receptors register the changes of the elongation of the vessels and transmit this information to medulla oblongata. With the received pressure informations initiates the medulla oblongata, if necessary, regulatory measures. For the short-term regulation is the sympathetic responsible. Both, middle-term and long-term regulation, is made by the kidneys. For middle-term regulation messenger substance are released, which entail vasoconstriction. The long-term regulation occurs per pressure diuresis or reabsorption in the kidneys. It is possible to measure different blood pressures at different places in the cardiovascular system, for example the mean arterial pressure (*MAP*). The *MAP* increases in relation to the stroke volume and decreases when blood flows into the peripheral system.[1, 7]

The cardiac output (*CO*) states the blood volume, which is pumped by the heart per time unit (*HR*). The calculation of the *CO* as follows.[1]

$$CO = HR \times \text{strokevolume} \quad (2.1)$$

2.2 Physical Base

To consider the hemodynamics, it is possible to draw conclusions by analogy of physical laws. Especially of Ohm's law $R = \frac{U}{I}$ or rather $I = \frac{U}{R}$. A special case of Ohm's law constitutes Hagen-Poiseuille's law in the field of fluid dynamic and rheology. Hagen-Poiseuille's law describes the laminar flow of an homogeneous Newtonian fluid through a rigid pipe depending on characteristics of the fluid and of the pipe.[8, 7]

Blood is an inhomogeneous suspension of liquid and corpuscular components, whose viscosity η depends on more factors than the temperature, and is consequently no Newtonian fluid. Nevertheless it is possible to draw conclusions by analogy out of Hagen-Poiseuille's law for the computation of the hemodynamics.[8, 7]

$$\frac{V}{t} = \frac{r^4 \times \pi \times \Delta P}{8 \times \eta \times I} \quad (2.2)$$

Chapter 2. Hemodynamics

Here is the volume flow equivalent to the electrical current I and the pressure difference ΔP to the electric voltage U . Thus, the calculation of the resistance as follows.[8, 7]

$$R = \frac{8 \times I \times \eta}{r^4} \quad (2.3)$$

Thereby volume flow increases 16 times and the resistance decreases 16 times for double radius r .[8, 7]

3 | Vasomotion in disease

This chapter describes pathologic incidents in the cardiovascular system and organs during shock.

In general shock is characterized by hypoxia in tissues due to inadequate blood supply. The hypoxia during a shock leads to the deposition of metabolisms in organs what results in a increased risk of multi organ dysfunction. There are four different types of shocks: [9, 10]

- **Hypovolaemic shock** is caused by a lack of volume. Either as a consequence of blood loss (hemorrhagic shock) or of water, plasma or electrolyte loss.
- **Cardiogenic shock** is caused by cardiac failure, for instance myocarditis, cardiomyopathy in final stage or acute myocardial infarction.
- **Obstructive shock** is caused by obstruction of blood flow, for instance pulmonary embolism, cardiac tamponade or tension pneumothorax
- **Distributive shock** covers, inter alia, septic shock, anaphylactic shock and neurogenic shock

Main cause for cardiogenic, hypovolaemic and obstructive shock is a decreased cardiac output without adapting the peripheral resistance. That leads to a lack of oxygen supply. Whereas the main cause for a distributive shock lies in a dysfunction of the peripheral areas in terms of reduced systemic vascular resistance as well as varied oxygen extraction. [10]

Shock affects alterations in the microcirculatory system what interferes the perfusion [11]. The changes in the circulatory system are in the following part further elaborated with the aid of sepsis.

Sepsis

Sepsis is a condition, that develops on behalf of systemic inflammatory response syndrome (SIRS) with presence of an infection or bacteria in the tissue, within the body which triggers an immune response. This response often overburdens the immune system, to fight the inflammation or bacteria. Some of the normal macrohaemodynamics of sepsis are abnormal body temperature, abnormal heart rate, oxygen extraction and abnormal blood pressure.[12, 13] Sepsis is often associated with three stages, sepsis, severe sepsis and septic shock. This is illustrated in figure 3.1.

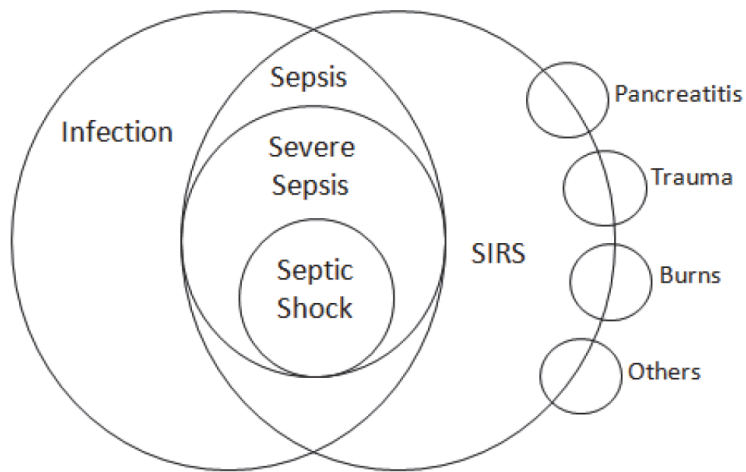


Figure 3.1: Relation between SIRS and infection. Showing the stages in sepsis and some of the causes of SIRS which include pancreatitis, trauma, burns etc.[13]

Stage 1: Sepsis

Under the stage of sepsis several things happen mainly at the capillary level, that leads to impaired homeostasis in the body. Bacteria which are responsible for causing irregularity are present in the blood and in the tissues around the vessels. Initially, when the body encounters an infection, white blood cells are recruited to release molecules which interact with the endothelial in the blood vessels will fight the infection. The interaction causes the vessels to dilate to increase the blood vessel diameter and permeability. The increased diameter slows down the blood flow, which causes a drop in blood pressure. Also the vessels permeability is increased. This reaction happens multiple places in the body where there is infected tissue present and will cause systemically vessel dilation. The characterization of sepsis is SIRS as a result of infection.[14, 13]

Stage 2: Severe sepsis

When the permeability of the vessels is increased, more fluid is in the tissue and the cells get less oxygen due to prolonged time for get to the demanding tissue. Also the endothelial of the vessels will get damaged when the white blood cells try to destroy the pathogens. This triggers coagulation and clotting is formed in the damaged areas in the blood vessels. At a point the damaged vessels leads to more leakage, because there will be a point where the coagulation cannot keep up. Organs will start to dysfunction at this stage. The characterization of severe sepsis is presence of sepsis with organ dysfunction and hypoperfusion is often included in this state. The mortality rate for patients with severe sepsis are about 25 to 30% [14, 13].

Stage 3: Septic shock

Septic shock occurs when the body has undergone sepsis for a greater duration of time. This stage is characterized by a condition with hypotension even after adequate fluid resuscitation is given. Because of lactic acidosis the cells are not getting a sufficient supply of oxygen and therefore the cells will begin to die. This can lead to a very dangerous state, where organs begin to fail because they get damaged to function. When multiple organs get damaged the state in septic shock reaches multiple organ failure also called multiple organ dysfunction syndrome (MODS)[14, 13]. The mortality for patients with septic shock are in the region of 40 to 70% [13].

4 | Methods of studying vasomotion

In the following chapter an introduction to different techniques of measuring vasomotion will be given. Here methods and applicability for measuring vasomotion will be presented, with main focus directed towards thermal imaging and important parameters using this technique.

For some time it has been the interest of researchers and health care clinicians to get a better understanding of the mechanisms that control and regulate local blood flow in the microcirculatory system[15, 16, 2, 17]. Visualization of the vessels in skin and the way these behave can be important for assessment of stages of sepsis as mentioned before in chapter 3, but also in peripheral vascular disease, the results of skin reconstructive surgery, wound and ulcer management.[17, 13] Spectral components of vasomotion seem to vary when influenced of some diseases. An example could be a decrease in amplitude of endothelial blood flow oscillations is assumed to be a biomarker for endothelial dysfunction. Endothelial dysfunction indicate cardiovascular disorders such as arterial hypertension and cardiac ischemia. An increased amplitude within the neurogenic frequency band is characterized by a decrease of vascular resistance and an increase of blood flow through the arteriovenous shunt.[16]

For measuring regulation in the peripheral blood flow, it is assumed that these oscillating changes are the source of thermal waves propagating from microvessels toward the skin surface. Especially thermal imaging uses this concept.[16] Furthermore a correlation between skin temperature in fingertips and blood flow oscillations has been found[15]. When the thermal waves propagate from the vessels towards the skin surface they are prone to some attenuation. This is due to skin properties that function like a low-frequency filter.[18] The magnitude of attenuation is directly proportional to the frequency. Therefore as illustrated in fig. 4.1, a higher frequency leads to a higher attenuation.

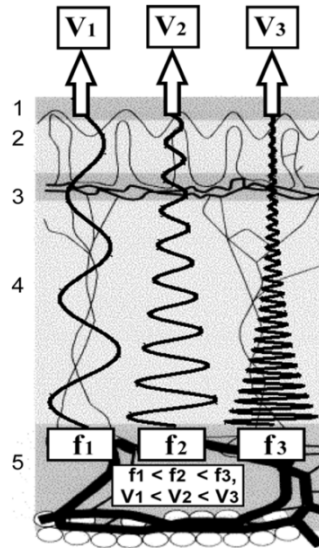


Figure 4.1: Graphical representation of amplitude dampening in three signals with different frequency.[15]

There are multiple different techniques of measuring blood flow in the peripheral circulatory system. For example capillaroscopy, laser Doppler flowmetry (LDF), and thermal imaging. These have been used differently trying to quantify functional aspects of skin vasculature.[17] Laser Doppler flowmetry is one of the most used[2] and thermal imaging being introduced as a new technique of measuring vasoregulation[15].

4.1 Thermal imaging

In studies made by a Russian group by Sagaidachnyi et al. thermal imaging has been used to study vasomotion. In their studies they sought to get better understanding of the relationship between blood flow oscillations and temperature oscillations, and if it was possible to recreate the blood flow oscillation from temperature recording. Recordings of flow were done by Photoplethysmography and temperature of the skin by thermal imaging. The recordings were made on a small point of the fingertip. Through their work, five frequency bands were identified as vasomotion activity, and are following: endothelial (0.005–0.02 Hz), neurogenic (0.02–0.05 Hz), myogenic (0.05–0.15 Hz), respiratory origin (0.15–0.4 Hz) and cardiac origin (0.4–2.0 Hz).[16, 15] The choice of using thermal imaging to study vasomotion implies certain advantages. Mainly a larger sample area, but also a higher temporal, (up to 105 fps) and spatial (2048×1536 pixels) resolution. In addition it is also a non invasive way of measuring vasomotion.[16]

4.2 Laser Doppler flowmetry

In an other study from Geyer et al. vasomotion is investigated through the use of laser Doppler flowmetry as recording technique. In the study vasoregulation variables are

sought quantified. LDF is a non invasive approach to measuring changes in vasomotion. The technique register changes in the depth of 1 mm, and works like Doppler ultrasound, utilizing the shift in frequency. Though instead of using ultrasonic waves, LDF uses light reflected from red blood cells. This study found the same frequency bands as Sagaidachnyi et al. with minimal difference. Data obtained were analyzed through spectral analysis. Wavelet transform was used instead of the most used fourier analysis, because wavelet analysis offered better resolution to reveal characteristics in the low frequency area.[2] LDF uses a small sample area and the laser probe allows a sampling area as small as 1 mm³.[19]

4.3 Summarizing

Both Geyer et al. and Sagaidachnyi et al. managed to show spectral components relating to vasomotion. The techniques both uses a non invasive approach, even though the methods are different when measuring red blood cell count compared to temperature. The use of thermal imaging as the method of measuring vasomotion offers interesting opportunities. Larger sampling area would allow interpretation and study of a more global tissue area. Along with the resolution of thermal imaging cameras, this makes thermal imaging the choice of measuring technique to be used in this study.

5 | Infrared Thermal Imaging

The following chapter will include an introduction to thermal imaging, where general concepts and physical principals will be explained. Furthermore it will be explained how a device measures infrared radiation.

5.1 Introduction to thermal imaging

Thermal imaging is an technique that utilizes infrared radiation emitted from nearly any objects. The existence of infrared radiation was first discovered in 1800 by Sir Frederick William Herschel. His experiments lead to the knowledge that there is a light spectrum beyond the visual spectrum humans are able to perceive. Any object above absolute zero emits energy-electromagnetic radiation depending on its temperature.[20, 21]

Infrared radiation is also known as thermal radiation because of the relationship between temperature and infrared radiation. Temperature of the human body permits radiation in the infrared spectrum, but objects of much higher temperature are capable of emitting radiation in the visible and UV spectrum. This has to do with the difference between object and environmental temperature. If the temperature of these are relatively close to each other, the radiation emitted will be within infrared wavelengths. Infrared radiation has a wavelength from 769 nm to 1 mm. Objects emit more radiation in some region regions compared to others. Because of this is the infrared spectrum classified in the three regions, near, middle and far infrared. Near is between 769 nm and $2.5 \mu\text{m}$, middle $2.5 \mu\text{m}$ to $50 \mu\text{m}$ and far $50 \mu\text{m}$ to 1 mm. The human body emits most radiation in the far infrared part, and most thermal cameras are build with this in mind. Near and middle cameras are used to measure gases.[20]

Thermal imaging is commonly used to calculate surface temperatures. Two important concepts, heat and temperature emerge in the understanding of this. Temperature is a measure for the internal energy within an object and can be defined as the average kinetic energy of the object. Heat is the energy that passes from a warm object to a colder object. Warm objects will decrease in internal energy and cold objects will increase due to the temperature difference and therefore the heat transfer. In the human body, a constant temperature is keep, due to several factors and therefore the temperature will not decrease even though a heat transfer to the surrounding environment occurs. The environmental temperature do have an impact on how large the heat transfer gradient is. If a body is in a cold environment, the emitted heat will be greater than the absorbed. In the same way, if the environment is much warmer than 37°C , a greater absorption than emission will occur and the body will increase in temperature.[20]

5.2 Measuring thermal energy

The theory of the black body is important to understand the absorption and emission of light relative to temperature. Because the theory of the black body is used to describe the laws of infrared radiation and its relationship to temperature. The black body is an ideal perfect emitter of infrared radiation because it absorbs all electromagnetic radiation permitted to it, and it emits the same amount of radiation as it absorbs, the absorption and emission are both equal to one. Spectral emissive power, also denoted E_λ is the energy emitted by a surface in relation to time and range of wavelength. Figure 5.1 shows an graphical illustration of spectral emissive power of the black body for specific wavelengths when the temperature changes. [20]

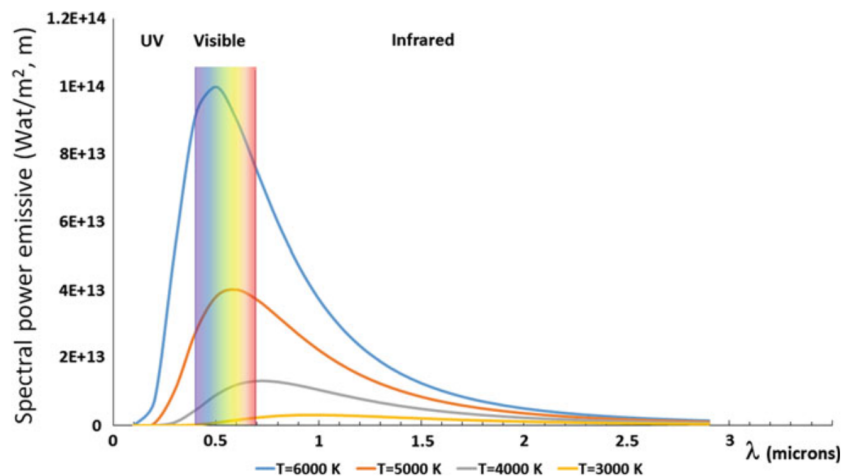


Figure 5.1: Spectral power emissive as a function of wavelength for different temperatures.[20]

The knowledge of this principle helps in the understanding of how infrared radiation behaves, and how temperature affects the wavelength of the signal. The radiation from the human body which has a temperature at 37°C emits the maximum energy of $9.3\mu\text{m}$, which means that most of the radiation is in the far infrared spectrum.[20]

Physical laws including Wien's displacement law and Stefan-Boltzmann's law are important for explaining how the infrared radiation behaves at different temperatures. [20]

Wien's displacement law explains that the wavelength of the peak of the black body radiation curve decreases as the body temperature increases. This law can be used to describe different wavelengths according to the temperature of the black body which emits the radiation. Wien's law has the following equation:

$$\lambda_{max} = \frac{a}{T} \quad (5.1)$$

a has a value of $2.897 \times 10^{-3} mK$ and denotes the Wien's displacement constant. T denotes the absolute temperature in kelvin. λ_{max} denotes the wavelength of emission peak with unit in meters.[20]

Stefan-Boltzmann's law explains that small changes in temperature will lead to big changes in emissive power. This is seen in Stefan-Boltzmann's equation because it states that the total emissive power is proportional to the fourth power of the absolute temperature. [20]

$$E = \varepsilon * \sigma * T^4 \quad (5.2)$$

In Stefan-Boltzmann's equation E denotes the total emissive power with unit W/m^2 . σ denotes the Stefan-Boltzmann's constant, and has a value of $5.67 \times 10^{-8} W/m^2 K^{-4}$. T is the temperature in kelvin. ε denotes the emissivity and is normally not a part of the Stefan-Boltzmann's law, but part of the modified Stefan-Boltzmann's equation, because it is used for calculation of temperature in most thermal cameras.

Emissivity is different for all materials. Skin have an emissivity between 0.95 to 0.99, why these values typically are used when assessing the temperature of the skin of the human body with thermal imaging. This law is important when considering thermal imaging because the sensitivity when calculating the temperature from the emissive power is considerable. [20]

Thermal cameras

Thermal cameras contain a lens to focus the electromagnetic radiation emitted by an object onto a detector element. A focal plan array (FPA) contains between 384×288 and 1024×768 microbolometers and is often used as detector element in uncooled thermal cameras.[22, 21] The thermal radiation focused by the lens warms up the microbolometers in the FPA. Since microbolometers contain temperature-dependent electric resistance, the voltage of the electrical outcome signal is depending on the detected radiation. The output is then undergoing amplification before further signal processing that digitalizes the signal into pixels. This allows the final output signal to be viewed as a temperature for the object on a monitor, this is also illustrated on figure 5.2. [21]

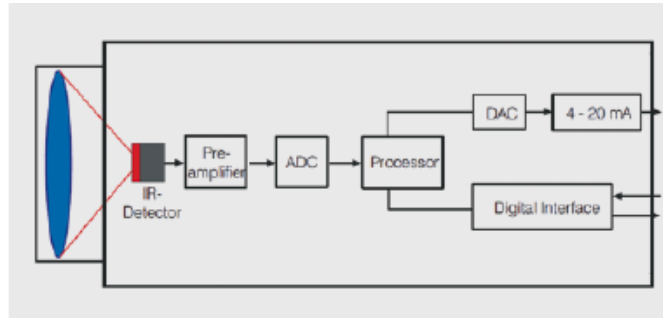


Figure 5.2: Simplified block diagram of an standard infrared camera.[21]

The infrared radiation is made into an electrical signal in the camera, this data can be used in calculating the temperature for an object by knowing certain variables and putting these into Stefan Boltzmann's equation 5.2. The emissive power denoted E , is the radiation that the detector in the camera is getting. The variables σ are known and ε is specified for the object that is being measured, eg. the human skin with emissivity between 0.95 to 0.99. The temperature are then the only variable to calculate and this is done for each pixel in the image to make up the complete thermal image of the object. Each pixel will be representing one thermal data. [20]

Part II

Methods

6 | Study setup

In this study the peripheral circulation is observed to investigate changes in microcirculation during partial occlusion of blood supply. Infrared imaging is used to measure the temperature changes in the skin of the hand, which is used as an indicator for peripheral circulation.

To see if there are changes in the microcirculatory system depending on flow to the observed area, the test is set in two conditions. The first measurement of the hand, is done with no intervention, and used as a control measurement. The second measurement of the hand is done during a partial occlusion of the blood supply. The partial occlusion of the arm leads to ischemia what leads to a lack of oxygen [1]. Aim of the study is to investigate, if there are measurable changes in the micro temperature oscillations of the skin caused by hypoxia in case of shock. Therefore the induced ischemia is used as a way to mimic hypoxia due to shock. The reason to do a 50% restriction of blood flow, is due to the intend of creating ischemia without forcing to much discomfort on test subjects, over the 20 min occlusion period. Discomfort test was done prior to the start of the experiment.

By first taking the control measurement under normal conditions, the carry-over effect of occlusion is avoided. It enables taking both measurements of each subject straight successively, which should reduce inaccuracies within the setup of both experiments for each subject. The setting was assembled in the Regionshospital Nordjylland in Hjørring.

6.1 Subjects

Four healthy subjects within the age of 22 - 52, three male and one female were recruited for this experiment. The experiment is done as a pilot study, why it is presumed that the sample size of four is sufficient. The research focuses on assessing the microvascular system with the hand as a window on healthy subjects. Specific inclusion and exclusion criteria have been formed for this experiment:

Inclusion criteria

- Subjects must be in a normal healthy condition
- Subjects must have at least one hand to perform the measure on
- The cuff must be able to fit the arm circumference
- The subject must be able to sit still over the 45 min. recording period

Exclusion criteria

- Health conditions that set the subject in risk of injury when conducting the exper-

- iment.
- Obesity to a greater extend
 - Diseases that triggers tremors

6.2 Test setting

The subject will be placed in a upholstered chair with adjustable backrest, footrest and armrests, which allows a good positioning of the measured hand, while the subject remain in a relaxed position. Measurement will be carried out on the dominant hand. The hand is stabilized with a vacuum pillow which is covered by a micro fiber tissue to get a better background for the images. Microfiber has a low heat conduction [23]. That helps to identify the outlines of the hand on the thermal image, because the tissue is not conducting the temperature of the hand to a high extent. To provide a more comfortable position of the arm during the experiment the armrest of the adjustable chair is padded with some sheets under the vacuum pillow. A comfortable position in the chair is important, because the subject has to sit still and is not allowed to move during the test for at least 45 min. These precautions only counteract some small movement, and therefore it is important that the subject is focused on sitting still. $37,5 \pm 1,0$ cm over the hand the Gobi 640 $17\mu\text{m}$ GigE infrared camera (Xenics NV, Belgium) is positioned with a tripod. The setup with camera, chair and computer can be seen on figure 6.1.



Figure 6.1: The test setting at the Regionshospital Nordjylland.

The camera is via a Ethernet cable connected with a laptop, which is used to record the measurements with Xeneth 2.6 software. First cable connections between the camera, the laptop and the power supply have to be set. Afterwards the camera is turned on and has to warm up for about 15 min. During this the laptop should be started and the software for taking the measurements is set in operational readiness.

When the preparation of the test setting is done, the preparation for the subject can begin. At first the blood pressure of the subject is measured on the dominant arm. The blood pressure is measured three times while the subject is sitting relaxed on a chair. Mean systolic blood pressures is calculated. To get the total occlusion pressure (*TOP*) the mean has to be multiplied by 1.3. To reduce the blood flow in the arm to 50% during the measurement within the second condition, the arm is cuffed with 30% of the *TOP*.[24] The cuff is then affixed at the subjects dominant arm without tighten it, so that it is ready for the second part of the experiment. After that the subject can take place in the chair and the hand can be stabled with the vacuum pillow. The vacuum generator is attached to the pillow for giving the hand more stability. The lens focus has to be adjusted so the distance is taking in to consideration, to make sure the image is sharp.

When the camera is stable and the filename is modified according to the subject, the first measurement can be started for 20 min. During the whole experiment the subject is not allowed to move or speak to minimize movement bias. Directly after the first measurement the cuff on the arm of the subject is tightened with the calculated value. The pressure of the cuff should be observed during the whole measurement and if necessary adjusted.

To guide the conductors of the experiment, an experimental protocol has been formed and to be followed during the experiment. The experimental protocol can be seen in chapter A.

6.3 Software setting

To interface the Xenics camera, Xeneth 2.6 software was used and settings were controlled from here. Sampling rate for the thermal imaging camera was set to the lowest possible at $50 * \frac{1}{8} Hz$ or $6.25 Hz$. This should be sufficient according to the Nyquist theory [25], when the frequencies of interest lies within $0.005 Hz - 2 Hz$ as presented in chapter 4. Ambient temperature and room temperature was set to 25° and emissivity to 1.

7 | Interpretation of data

The following chapter will contain information about the techniques that is used for the data analysis. The wavelet transformation will be used for looking at features to be used for the statistics where the paired t-test will be the approach

7.1 Continuous wavelet transformation

Analysis of the collected data from the thermal camera will be done in the time frequency domain. For this the wavelet transformation will be used to look for specific frequency content in the data. Wavelet transformation is practical when looking for signals of lower frequencies compared to the normal Fourier analysis, because of the bigger resolution in the wavelet analysis. Another drawback of the Fourier transform is the loss of time information, which is preserved with the wavelet transformation. [2]

Both the discrete and the continuous wavelet transformation can be used, but the continuous wavelet transformation has better resolution, why this is being used for interpreting the data.[2]

The continuous wavelet transformation is using a variable sized region windowing technique. Long time intervals are used where low frequency information is computed and short time intervals are used where high frequency information is computed. This is represented in figure 7.1.

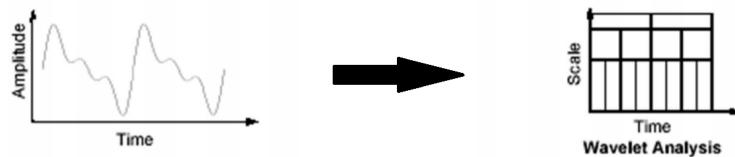


Figure 7.1: Signal to wavelet computation. Modified from [26].

The wavelet transform computes both the scale (s) and position (p) for the wavelet transform.

$$C(s, p) = \int_{-\infty}^{\infty} f(t)\Psi(s, p)dt \quad (7.1)$$

To achieve the continuous wavelet transformation, equation 7.1, the signal $f(t)$ is convoluted with the wavelet Ψ to get the wavelet coefficients for s and p .

This is done by computing the wavelet of the signal which then is compared to the wavelet for a section at the beginning of the signal. Then C in equation 7.1 is calculated for the section of the signal. The wavelet is shifted to the right and repeated until the entire signal is covered. Then the wavelet is scaled and C is computed for the entire signal again for all scales. [26]

Different wavelets can be used to compute the wavelet transformation. In Matlab the default is the Morlet wavelet.

The general form of the continuous wavelet transform is stated in equation 7.2:

$$W(t, s) = \int_{-\infty}^{\infty} \frac{1}{s^n} \psi * \left(\frac{\tau - t}{s}\right) x(\tau) d\tau \quad (7.2)$$

Where $\psi * \left(\frac{\tau - t}{s}\right)$ is the wavelet and $x(\tau)$ is the signal.[26, 27]

The signal or function is put into the continuous wavelet transformation equation 7.2. The wavelet transform will give a scalogram as an output. In Matlab the function CWT can be used to compute the continuous wavelet transformation by inserting the signal and the sampling frequency. This will give a scalogram as shown in figure 7.2. [28] The frequencies in Hz are shown along the y-axis if the sampling frequency is specified, else it will show the normalized frequency in cycles pr. sample. Along the x-axis is the time vector. The scalogram shows the magnitude of the signal to show how the frequency in the signal is distributed. A scale to see the size of the magnitude is also implied.

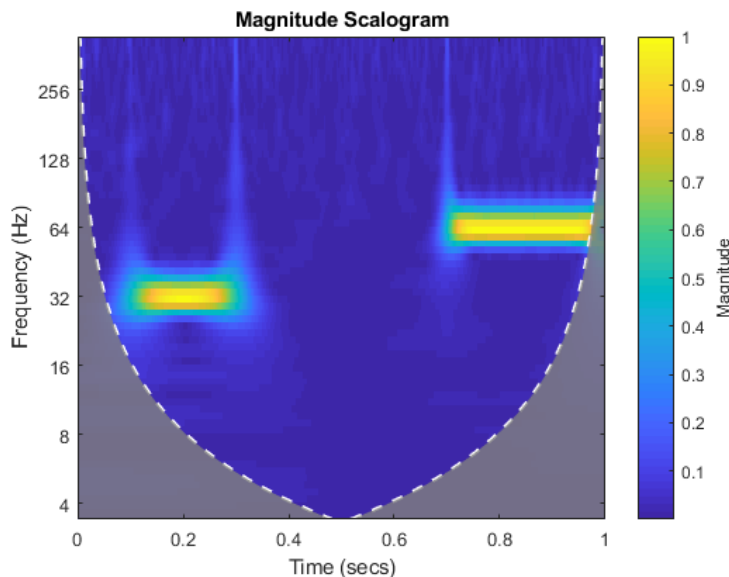


Figure 7.2: An example of a scalogram, showing frequency content at 32 Hz at time approx. 0.2 sec and 64 Hz at approx. 0.8 sec. [28]

The signal of the wavelet is typically of a finite length, which sets some limitations to the CWT, like the edge effect. The cone of influence (COI) shows the regions of the CWT where edge effects become significant. The gray zone are the areas where the edge effects become significant, which means that there will be some uncertainties to the CWT in this zone. [math]¹

¹FiXme Note: mathworks2017??

Part III

Data analysis

8 | Preparation of the data

Before any analysis of the acquired data could begin, it was necessary to load and extract the content of the xvi files produced by the thermal camera.

8.1 Dividing the data into frames

Data acquired from the thermal camera using the Xeneth 2.6 software is saved as an xvi file. These files were loaded and read into Matlab R2017b as an uint16 vector file. Before the frames could be separated from the xvi file, the header in front of the files needed to be excluded. The header contained 307729 data points. With the header removed, the frame separation could be carried out. This was done by first calculating the size of one frame. When knowing that each frame would have the dimensions of 640x480 pixels, the size of one frame would correspond to 307200 data points for each frame. It should be noticed that each frame also contained a 16 bit header, so this should be added to the size of each frame. The number of frames was calculated by dividing the length of one frame by the entire length of the data file containing all frames, without the file header. By this calculation it was known how many frames the file contained. The data points for each frame were trimmed for its specific frame header and reshaped from a vector into a matrix and verified by showing the images. The images contain the pixel intensities of values from 0 to 65535, which is correspondent to the size of the uint16 bit file.



Figure 8.1: Image of one frame from subject 1 after separation.

8.2 Regions of interest

The regions of interest (ROIs) were chosen as pixel locations in the image on specific places of the hand. ROI were selected on behalf of getting a full representation of the hand. Regions in the fingertips and nail folds are areas where it is easy to access the microcirculatory hemodynamics of the human body according to [29]. This region should therefore be expected to give some information on the changes in capillaries which can be an effect of vasomotion.

The original image on figure 8.1 is showing the hand but not with very good contrast. To easier choose ROIs, the original image was converted to a gray scale image to improve the contrast in the image, this can be seen in figure 8.2.

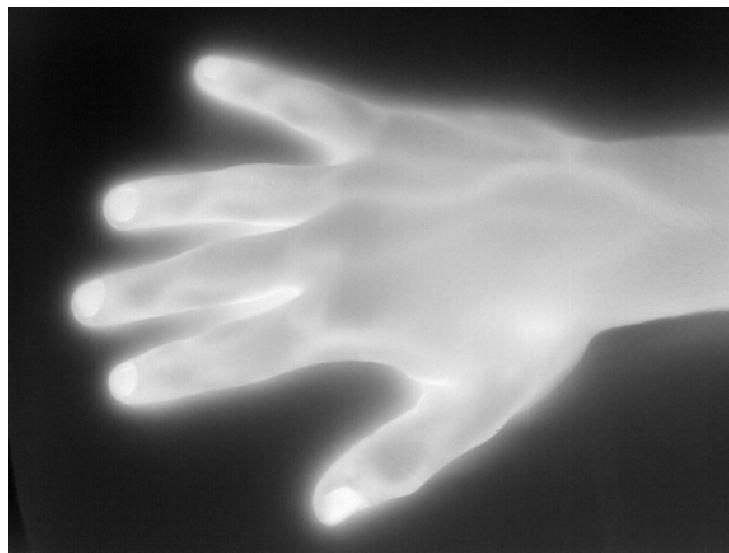


Figure 8.2: High contrast thermal image for subject 1.

With the improved contrast, 28 ROIs from the hand were chosen on the first image of the thermal image series, by finding the coordinates of the pixels on the image. The regions are illustrated on figure 8.3. The localization of the regions is originating from the fingertips and elongating down the hand to the beginning of the wrist. Each region gives an pixel intensity value from one pixel of the image. In the setup of this study one pixel corresponds to an area on the hand with a diameter of about $17\mu\text{m}$. Based on the fact, that the capillaries have an average diameter of $8\mu\text{m}$ [1], it is sufficient to represent each region with just one pixel. Even the area represented by one pixel contains more than one capillary.

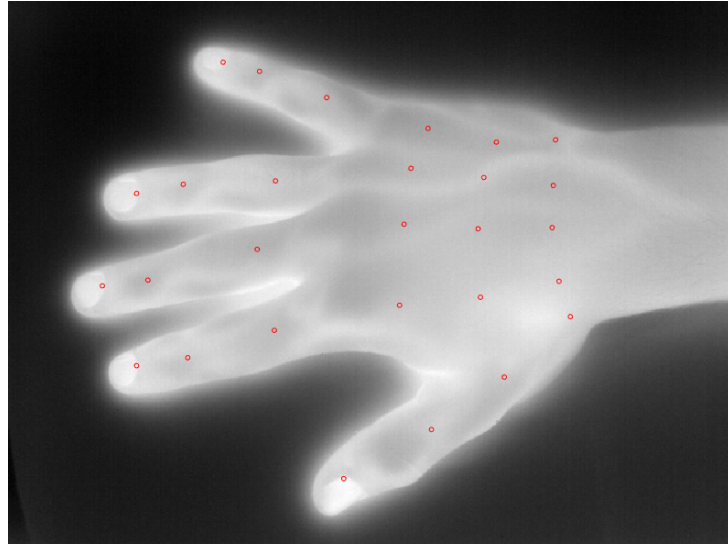


Figure 8.3: First thermal image of the uncuffed subject 1's uncuffed recording, with ROI of interest plotted on 28 areas of the hand represented as red circles.

The regions are fixed within the image matrix for the whole image series for each measurement, assuming that the subject was sitting still during the whole measurement. The regions also account for both the uncuffed and cuffed conditions for each subject, assuming that the position of the hand was at the same position in both conditions. Iterating over the image series saving ROIs into a cell array with data points for each ROI, a vector for each of the 28 ROI was made to give the pixel intensity variations over the whole measurement. An example of the pixel intensities for subject 1 is shown on figure figure 8.4.

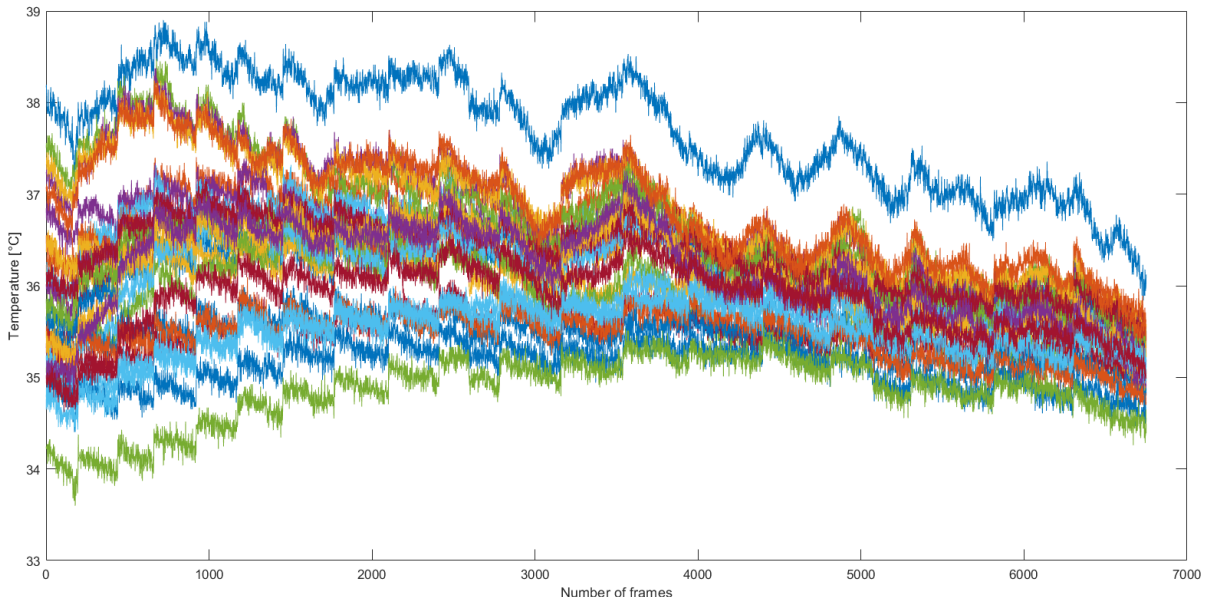


Figure 8.4: Pixel intensity for all 28 ROIs during the uncuffed measurement of subject 1.

8.3 Artifacts in temperature recording

As seen in figure 8.4 the data contain systematic changes which rule out a representation natural temperature variation. Since those changes occur at the same time in different locations of the thermal image, it is assumed that the greater shifts are due to a technological limit. Because of this assumption, it is chosen to further investigate the buildup of thermal cameras and look into other papers, to see if they had encountered similar difficulties.

8.3.1 Thermal pixel drift

In a study by Eriksen et al. where thermal imaging was assessed as use for measuring temperature of electrical systems, data recording showed similar behavior as recording in this study. They clearly state that two types of noise is present in their recording. One being white noise from the radiation detector and electronics, and another being a low frequency technical noise. To compensate for these artifacts, a moving average filter was applied.[30] A moving average filter would not be an appropriate correction method, because of the risk of loosing the low frequent content of interest.

Thermal cameras are composed of a matrix of microbolometers as mentioned in section section 5.2. Each microbolometer is also known as a pixel detector for thermal radiation.[22, 31] Unfortunately it shows that these microbolometers are really sensitive to noise especially in uncooled cameras, where the internal temperature is not regulated. The noise is formed because each microbolometer has a different response to the same infrared excitation. Furthermore it is assumed by some, that this response changes linear[22]. This drift in each microbolometer in the focal plane array is also known as non-uniformity. To achieve radiometric precision the camera has to make a correction for this drift called non-uniformity correction. A common way to recalibrate bolometers is to move a shutter in between the lens and the focal plane array. The shutter has a uniform color which is used to create a new reference for all microbolometers.[22, 31] These auto-adjustments might be what Eriksen et al. saw in their recordings.

Furthermore the drift component is increasing with increasing distance from the center of the thermal image.¹

8.4 Correction method

With the knowledge of what might be the source of the artifacts seen in the temperature recording, it is chosen to find a way to compensate and correct the recording. Jumps occur in each region of interest at the same time and are shown by a high difference of the values between two frames. The amount of the observed jumps varies between 0 and 20 in the recordings. Furthermore the appearance of the jumps is non-periodic and in each

¹FiXme Note: Reference needed.

recording at different time points and interval.

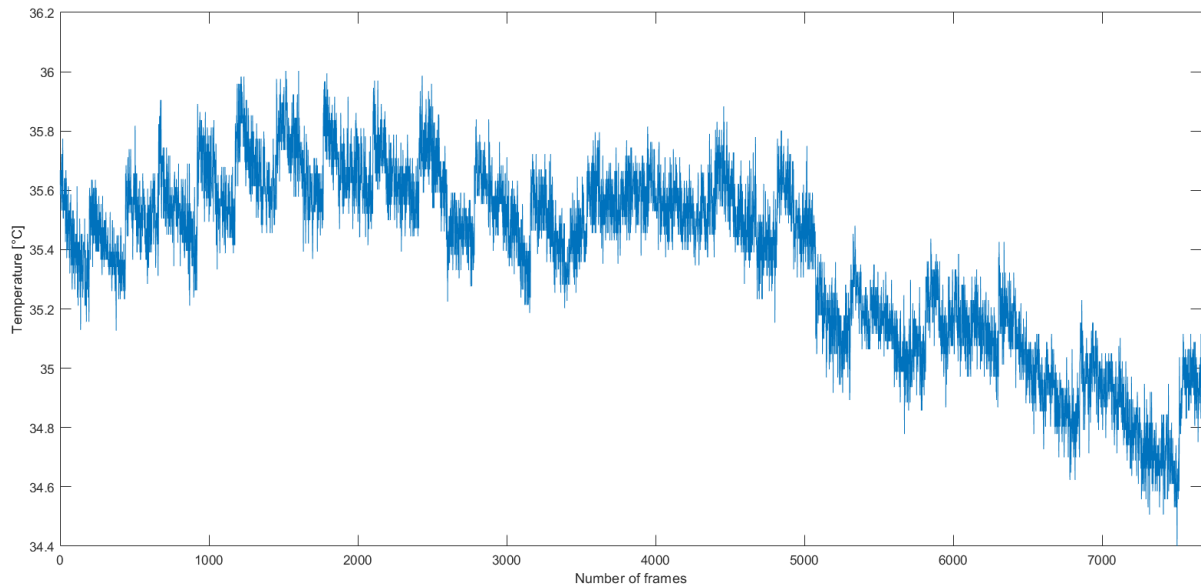


Figure 8.5: The original data of region 15 in the uncuffed recording of subject 1 including 20 jumps.

From the raw data magnitude of the scalogram show high magnitude peaks exactly at the same time points where the jumps are occurring, which can be seen in figure 9.1. Due to this falsifying of the magnitude, the results of the data analysis are also falsified.²

Additionally there is also a drift occurring within each interval between two jumps, which hampers the correct data analysis, this can also be seen in figure 9.1 as the frequency band with higher magnitude. To reduce the drift component and the jumps in the signals, the two following correction methods have been compiled, whereby the second one has been implemented.

Method 1: Regression of first interval

The first implemented method is based on the assumption that the drift is equal in each interval. It is also assumed that the thermal camera has been calibrated just before the recording, so the first interval can be used as a reference to calculate the drift component. Therefore a linear regression for the first interval has been made. With the resultant slope m follows the calculation of the drift difference d within the first interval. Due to the assumption, that the drift difference is equal, the slope of the drift of each interval depends on the length of the interval. The slopes have been calculated with equation 8.1.

$$m = \frac{d}{\text{length(interval)}} \quad (8.1)$$

²Fixme Note: We cannot ref to a figure that comes 4 pages later...

To compensate for the drift, a straight with the inverse slope and starting point in the first data point of the interval has been calculated. The middle points between the original data and the new calculated straight build the correction of the data signal.

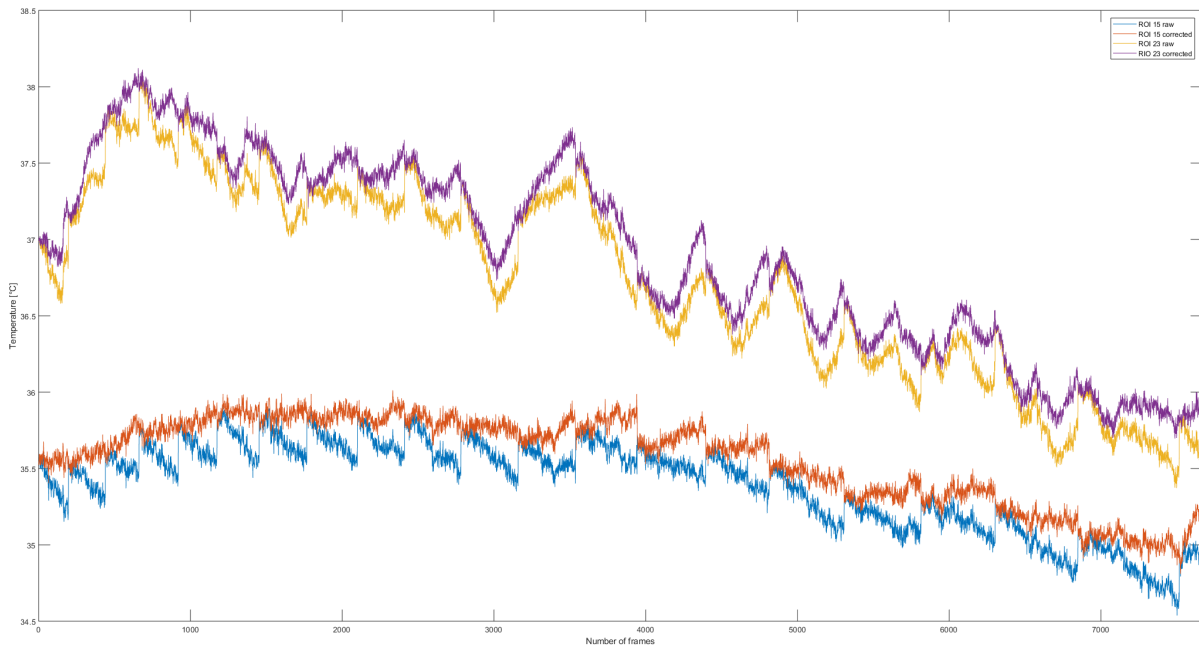


Figure 8.6: The original data of ROI 15 in blue and ROI 23 in yellow. Applied correction of ROI 15's data in red and ROI 23's data in purple.

As it can be seen in figure 8.6 this correction only worked partially where several parts showed less drift and lower jumps. Through the method worked at some parts it still had a lot of weak points. Primarily because some jumps had been strengthened. Due to the outcome of this method, the assumption, that the drift is equal in each interval has been discarded.

Method 2: Regression of each interval

The second implemented method is due to the failure of the first method based on the assumption that the drift is not equal in each interval. Out of the recorded data the exact drift is indeterminable. Hence a method which tries to fit the separate intervals together without the necessity of the awareness of the real drift component and avoids the suppression of the basic shape of the signal has been chosen. Therefore firstly the linear regressions for all intervals and the corresponding residuals are calculated. The idea is to move the end point of a regression line and the start point of the next regression line together. Thus the middle points between end and following start point are calculated. The alignment of the regression lines is changed, so that the start and end points of all the new created orientation straights fit the middle points, except the first and the last orientation straight. Both fit just one middle point. The start of the first orientation

straight is the start point of the regression line of the first interval and the end point of the last orientation straight is the end point of the regression line of the last interval.

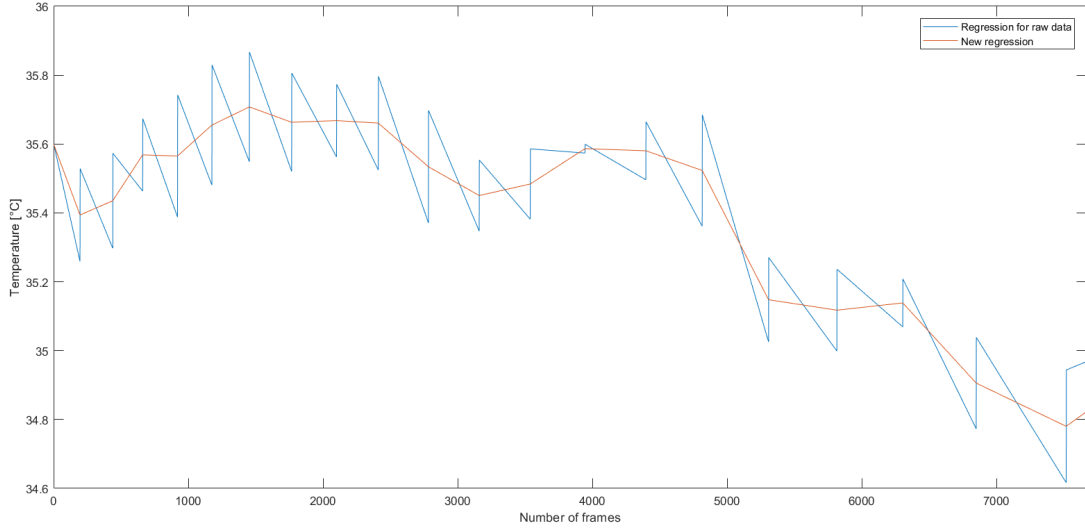


Figure 8.7: Connected regression lines of the original data of region 15 in the uncuffed recording of subject 1 in blue. New created orientation line of the same recording in the same region shown in red.

As shown in figure 8.7 the new orientation straight fits the regression lines together without suppressing the shape of the signal. Subsequently the residuals have been added to the new orientation straight, to sustain the ratio between the data points. Figure 8.8 shows the corrected signal wherein the jumps, separated intervals, have been connected and the jumps have been largely corrected.

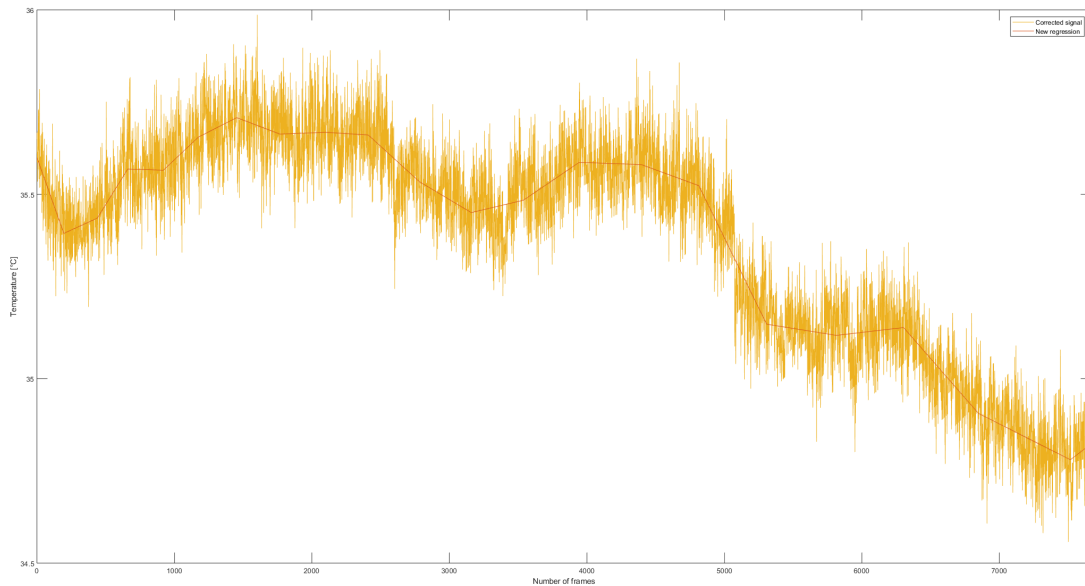


Figure 8.8: Orientation line based on the data of the uncuffed recording of subject 1 in region 15 shown in red. Corrected signal of the same data in yellow.

Chapter 8. Preparation of the data

However, this method still has weak points. In figures 8.5 - 8.8 region of interest is located in the center of the thermal image. Regions which are located in the outer area of the thermal image show a few jumps after the correction which are bigger than before, illustrated on figure 8.9. These extended jumps are due to the fact that the thermal image is more unstable in the outer areas than in the center, thus the pixel drift is increasing with increasing distance to the center of the thermal image. That means that in the corrected data of ROIs located in the outer areas of the thermal image still artifacts occur.

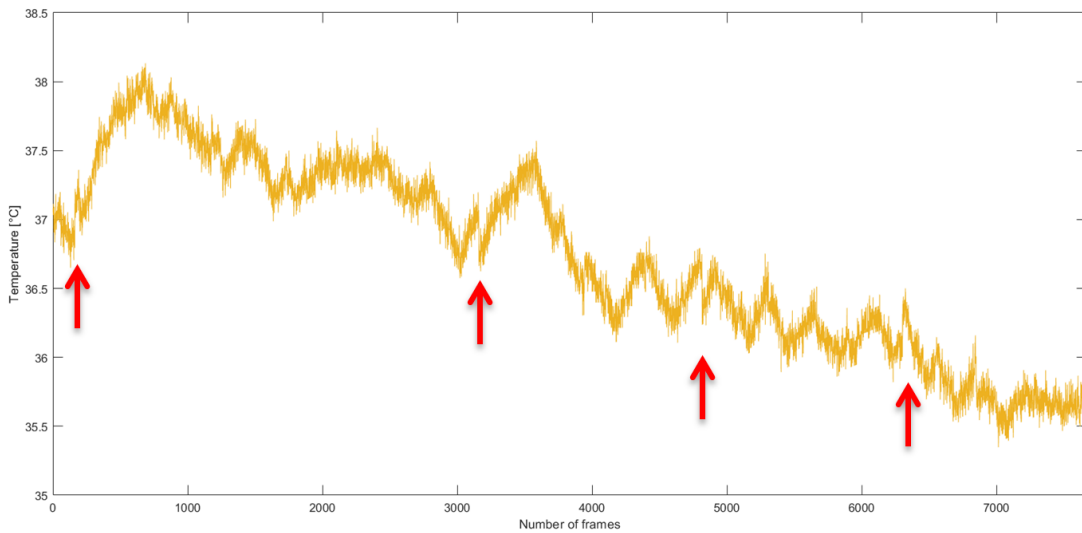


Figure 8.9: Corrected data of the uncuffed recording of subject 1 in region 23 shown in yellow. Red arrows show the jumps in this signal.

9 | Data processing

In this chapter the interpretation of the data from the corrected signal will be described. This interpretation will contribute to the values that will be used for the statistical test to see if the hypothesis will be rejected or not.

9.1 Scalogram interpretation

The data contains the time series of pixel intensities for each of the 28 ROIs for each recording of a subject which the CWT is computed for after the signal has been corrected. A scalogram showing the time-frequency analysis content of the signal is given as output of the CWT. Frequencies of higher magnitude will show up with brighter colors, which can also be seen on the magnitude colorbar for comparison of the magnitude with related values. The frequency illustrated by the scalograms lies between 2.7370 Hz and 0.0031 Hz. This means, according to the literature, that bands of cardiac, respiratory, endothelial, myogenic and neurogenic is represented in the wavelet frequency span for the time frequency analysis. [2, 15]

The scalogram in figure 9.1 is representing the CWT of the raw signal for ROI 8 from subject 3.

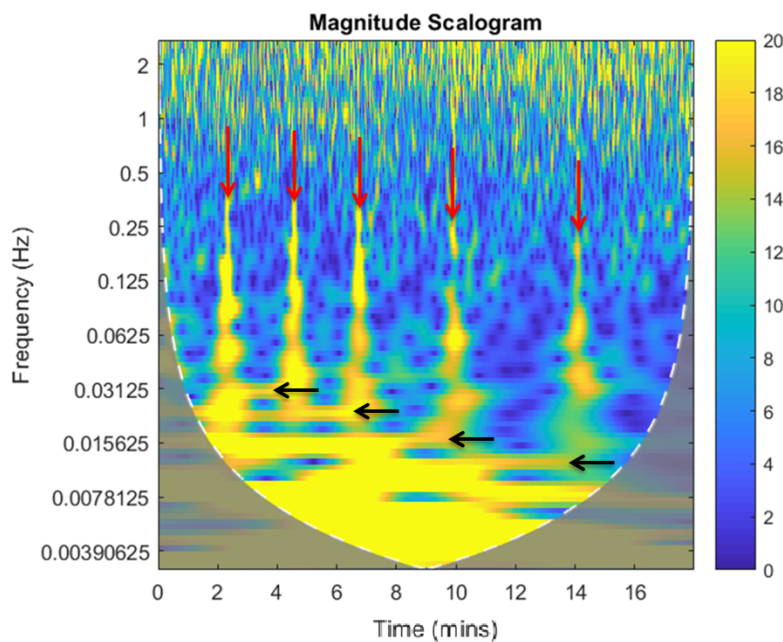


Figure 9.1: Scalogram from the raw data from ROI 8 in the uncuffed recording of subject 3. Red arrows mark high spikes. Black arrows mark drifts within the intervals.

Chapter 9. Data processing

Looking at the scalogram from the raw signal in figure 9.1 the jumps can easily be seen as the high bright spikes which represent the jumps in the signal. Five jumps that are indicated with the red arrows, are present in the scalogram at time points around 2.5, 4.5, 6.5, 10 and 14 minute time point in the signal. The jumps in the same signal shown in the time domain occur in the scalogram at the same time points. It is presumed that the corrected drift also is represented in the scalogram as low frequency content. Hereby different artifact components can be suspected to be included in the signal content.

The artifact components of the raw signal can be sorted into three categories:

- Uniform white noise artifacts
- Drift artifacts within each interval
- Jumps artifacts

Uniform white noise artifacts is characterized by having the same magnitude in all frequencies. This artifact will therefore not affect the signal of interest, because it will have a flat power spectral density throughout the bandwidth of the frequencies, because the signal of the white noise are independent and evenly distributed [32]. The jumps in the signal is induces by the auto-adjustments from the camera described in 8.3. The drift artifacts can be seen as magnitudes in the scalogram as lower frequencies than the jumps. A frequency band leading up to a high spike occur with each jump indicated with black arrows arrow in figure 9.1, indicating that the drift is not uniform between intervals. The artifact components will be disturbing the presumed signal from the micro oscillations to get a representative CWT, because this signal can be hidden by the artifacts. The artifacts are not constant for each recording, why the correction of the signal has been implemented.

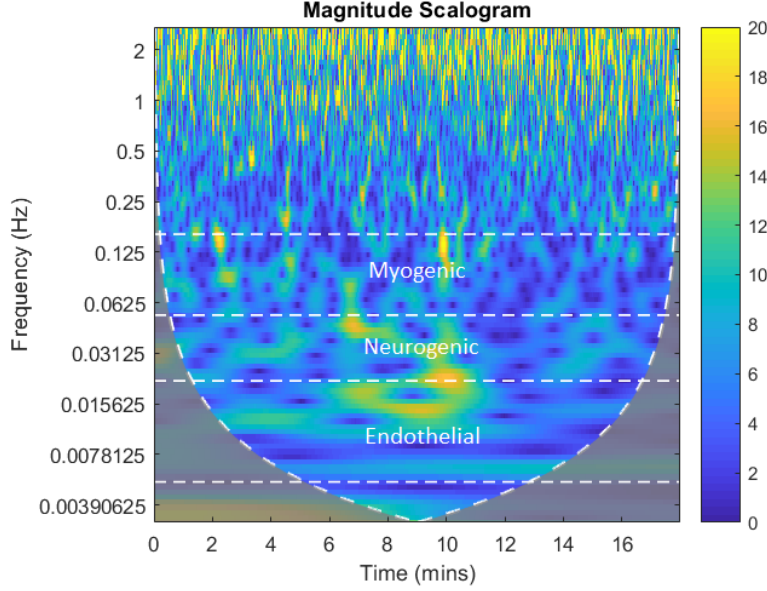


Figure 9.2: Scalogram from the corrected data of ROI 8 in the uncuffed recording of subject 3, where a dampening of the spikes and induced by the jumps has been achieved.

After the correction of the signal, the energy has been reduced in the areas induced from the jumps and the drift. The scalogram is left with less energy overall as seen in figure 9.2.

The three frequency bands are divided by white dashed lines in the scalogram seen in figure 9.2. To prepare the data for the statistical test, the average magnitude for each time period of each frequency band is first calculated by equation 9.1.

$$W(n_f) = \frac{1}{N} \sum_{n=1}^N W_n(n_f) \quad (9.1)$$

Where N denotes the total number of elements in the frequency band, W is the magnitude of the wavelet, n_f is the respective frame and n is the current element of the magnitude of the frequency band.

Then the mean of the average magnitude over the time period is calculated by equation 9.2

$$W_{mean} = \frac{1}{N_f} \sum_{n_f=1}^{N_f} W(n_f) \quad (9.2)$$

Where W_{mean} denotes the mean value of the frequency band over the time period and N_f is the total number of frames. This gives a single value for the specific frequency band to use in the statistical test for comparison between the two conditions.

9.2 Selecting ROIs for statistical test

After application of the correction method contain the signals of some ROIs still jumps what makes them for further data processing useless. Therefore each signal and its scalogram has been submitted a visual control. A table (Appendix) was used to evaluate each region in each subject within both conditions concerning the appearance of jumps after applied correction method and usability regarding further data processing.

With the aid of this evaluation table five ROIs have been chosen to use. The criterion for this selection was, that those ROIs showed in measurements good response to the correction method. All five ROIs are located in the back of the hand.

9.3 Statistical approach

As the actual distribution of the data is unknown, the statistical approach is based on the assumption that the data is normal distributed due to natural variance within subjects.

To test if there is a statistical significant difference between the uncuffed and cuffed condition a paired t-test is applied on the outcome data from the scalograms. The approach builds on using the total mean of each frequency band, condensing these down to just one number for each frequency band for one ROI for one subject, the approach of the calculation is explained in 9.1. Before a paired t-test is computed for the data, a boxplot is of the data is shown to get a visual representation of the data of the three frequency bands.

A paired t-test will be performed on all five regions, where uncuffed is the before condition and cuffed is the after condition. The outcome of the paired t-test will either be rejecting the h_0 hypothesis, that there is no difference between the two conditions, or not rejecting the h_0 hypothesis, which indicates that there is a difference.

The significance level of 0.005 is used the statistical test. This measures the likelihood of rejecting h_0 when it is true, which will lead to a type 1 error. The 0.005 significance level presumes that there is a 5% risk of concluding the sample mean to fall within the critical region at the level of 0.005 and thereby concluding the wrong assumption. [33]

Part IV

Results

10 | Results

In this chapter the results on behalf of the data analysis will be shown. A Wilcoxon signed rank test of the mean magnitude for each frequency band specified in 4.1 is computed to test the likelihood of finding a difference between the uncuffed and cuffed conditions.

10.1 Wilcoxon signed rank test

The boxplots can be seen in figure 10.1 throughout figure 10.3. The boxplots show points for each mean magnitude for each subject ordered by color, a line is connecting the before and after condition to indicate if there has been an increase or decrease in magnitude.

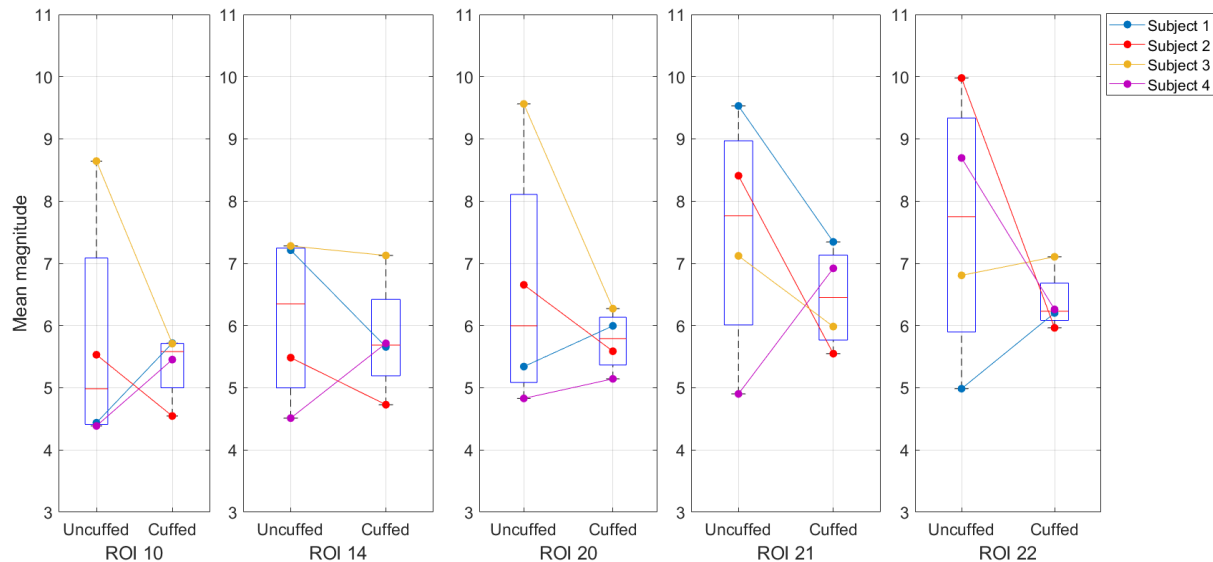


Figure 10.1: Boxplot for mean magnitude in the endothelial frequency band, for both conditions in five ROIs.

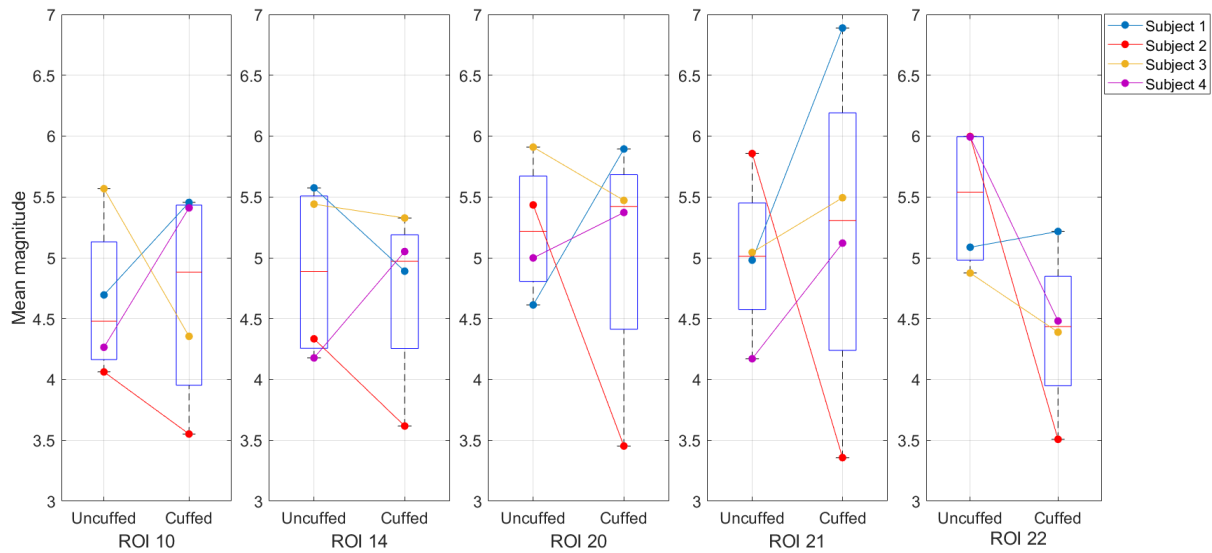


Figure 10.2: Boxplot for mean magnitude in the neurogenic frequency band, for both conditions in five ROIs.

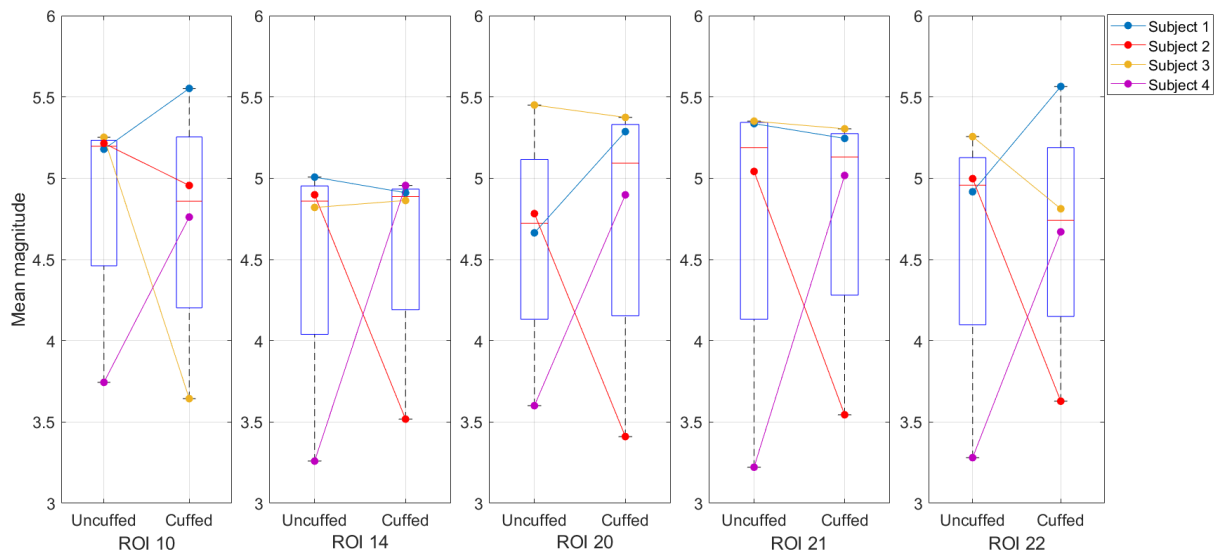


Figure 10.3: Boxplot for mean magnitude in the myogenic frequency band, for both conditions in five ROIs.

The outcome of the Wilcoxon signed rank test is a table showing the p-values, which is shown in 10.1.

Chapter 10. Results

Table 10.1: Table showing the p-values corresponding to specific ROI in correlation with frequency band.

	P-endo	P-myo	P-neuro
ROI 10	1	1	1
ROI 14	0.6250	1	0.8750
ROI 20	0.6250	1	0.8750
ROI 21	0.3750	0.8750	0.8750
ROI 22	0.6250	0.8750	0.2500

As indicated in table 10.1, all of the tests show a significance level well above 0.005, which means that h_0 is not rejected, whereby there is no difference between the two conditions. When reflecting the p-values onto the boxplots the correlation between the p-values and the occurrence of a difference in the dataset can be seen. For instance the lowest p-value of 0.1552 indicates the greatest difference between means, this can also be seen in figure figure 10.2 for ROI 22.

Part V

Discussion

11 | Discussion

The present study used thermal imaging to detect if there are measurable changes in the micro temperature oscillations of skin depending on blood flow to the observed area of the hand. Whereby the temperature changes in the skin were used as indicator for vasomotoric activity. The means of the regarded frequency bands in both conditions resemble one another. Hence the results of the paired t-test of the regarded frequency band means show no clear significance.

Reasons for insignificant results

The obvious assumption that there are no changes in the microcirculatory system or rather in vasomotion by 50% restriction of blood flow can be substantiated by independence of the microcirculatory system. Though the assumption of independency can be excluded because the available amount of blood in the microcirculatory system is dependent on the amount of blood the macrocirculatory system provides, which means that the microcirculatory system is not independent. Another explanation for the insignificant result would be by incorrect brachial occlusion. Incorrect occlusion would yield insufficient restriction for affecting the microcirculatory system. A wrong occlusion pressure could be the cause of this. As it can be seen in table A, the blood pressure measurements of three subjects delivered high values around 140mmHg and around 150mmHg . Since those three subject were in different age and shape, a suspicion for incorrect values arise. Even if the blood pressure monitor delivered wrongly high values, the outcome of the second measurement would not have been influenced negatively. This would only lead to a calculated occlusion pressure higher than the one needed to reach the intended restriction, which would just lead to a larger difference between both conditions. It would be more problematic with a occlusion level to low.

The small sample size of four subjects applied to the statistical methods are not sufficiently meaningful. With a larger amount of subjects this study would get a more meaningful result. A larger amount of subjects might therefore have provided a significant difference between both conditions. An even gender distribution might also have been preferable. But regarding the measured data there cannot be seen a clear difference between female and male subjects. Furthermore the missing randomization of the study design can be criticized. Though in the case of this study it was not possible to randomize which measurement is conducted first. If the condition with 50% restriction of the blood flow would have been carried out first, the data of the measurement under normal conditions would have been affected by a carry over effect. A randomization could possibly have been carried out by measuring one condition one day and the other the next day, and made sure when picking out ROI that it is the same locations on the hand in the data processing part. It should also be considered if there is an effect of the hand just lying still. For instance subject 2 and 3 had cold hands in the beginning of the experiment and got progressively warmer as the experiment went on. There might be a need for an

habitation period for the hand, but this would have to be investigated further. However this study was used as a pilot study to investigate if thermal imaging can be used to detect vasomotoric activity. Also impaired by subsequent elaborated limitations it would not have been worthwhile to recruit a larger amount of subjects even though it was the first intention.

Results

The mean values that the Wilcoxon sign rank test is based on, are extracted from the cwt data in the specific frequency bands. Though the COI has not been taken into consideration. This might be preferable to exclude, because the data outside of the COI is containing areas where the edge effect is significant and these data might not be representative for the result. A way this could have been achieved was by generating a mask to collect the data inside the COI. By excluding the data outside of COI it might have lead to different results, but this is doubtful.

The approach of the statistical test is a Wilcoxon sign rank test to test for significance differences within the dataset. This method is mainly used because of the study design, where it is determined if there is a difference before and after two conditions, within each subject. It is assumed, with the small sample size, that the data is non-normally distributed, why a non-parametric test is used. If the case of a normal distribution is present the paired t-test would be the approach for the statistical test. This test require a normal distribution in the population and is focusing on the population mean and not the median value like the Willcoxon signed rank test[34].

Limitations in the setup

The used thermal camera of uncooled type induced jumps and pixel drift within the intervals between each jump. Therefore a correction method was implemented, which clearly affects parts of the signal in specific ROIs. The pixel drift increases with increasing distance to the center of the thermal image why pixel drift of ROIs located in the outer areas of the thermal image cannot be completely compensated for with the implemented correction method. The explanation for this is likely that the correction method is based on the assumption that the drift component in every interval is linear. This assumption might be wrong and a correction method that uses another regression method or combines different regression methods might adjust the artifacts in a better way. As a result the ROIs located in the outer area of the thermal image were excluded from the data analysis. Another camera might also be preferable to reduce the risks of technical artifacts like these.

Vasomotoric activities measured by other studies where done in the fingertips [35, 15]. Whereas this study compared just areas on the back of the hand based on the assumption that vasomotoric activity can be measured equally in every area of hands skin. The results lead to the suspicion that vasomotoric activity cannot be measured equally on the back of the hand and the fingertips. The reason for not taking the fingertips into account is the uselessness of the data in these areas. Key reasons are the properties of the thermal

Chapter 11. Discussion

camera. Since the thermal pixel drift is known the regions of most interest should be centered in the thermal image.

Furthermore the smaller the observed area the closer the thermal camera has to be to this area. Thus the area represented by one pixel gets smaller. Within this study one pixel represents an area with a diameter around $417\mu m$. Whereas previous studies observed smaller areas which means that the pixel represent a smaller area. With the use of a larger ROI, it might be that the amount of inverse dilating capillaries is equal and thereby canceling each other out. Due to inverse dilating capillaries there might be no changes over time measurable because the frequency contents are occurring alternating in the different capillaries. In addition, it is obvious that the artifacts content in the signal is significantly higher than in the temperature signals detected in previous studies. Comparing the signals the question arises if the artifacts overlaps or suppresses the frequency content of vasomotoric activity. Even though temperature changes over time in the skin were detected, it is uncertain, if this signal just represents the general skin temperature or also vasomotoric activity.

Other limitations might be that the subjects hands had to be stabilized by a vacuum pillow with the assumption the subjects were still, but this does not give sufficient support to inhibit every movements of the subject. A mechanism for better stabilization of the hands should be included. An approach to compensate for instability of the hand during the experiment could have been to include image alignment in the data processing to limit the drawbacks of possible movements in the recordings. Furthermore with the used setup exact same conditions for each subject cannot be granted. For instance the room temperature should have been measured beforehand and taken into consideration before the start of each experiment to create the same conditions for all subjects. The presetting of the room temperature might have affected the data. This suspicion is enhanced by regarding subject 1's hand temperature which was $38^\circ C$. Also by regarding the hand temperature of $26^\circ C$ of subjects 2 and 3, who had cold hands during the measurement, this suspicion is enhanced. The software settings should be verified and if necessary changed beforehand of the experiment.

An optimization of the test setting would require a more controlled setup of the experiment and a thermal camera of higher quality preferable of a cooled type would have improved the validity of this study.

Bibliography

- [1] Bartholomwe EF Martini FH, Nath JL. *Fundamentals of Anatomy and Physiology Ninth Edition*. Pearson, 2012, p. 1272. ISBN: 13: 978-0-321-70933-2.
- [2] Mary Jo Geyer et al. “Using wavelet analysis to characterize the thermoregulatory mechanisms of sacral skin blood flow.” In: *Journal of rehabilitation research and development* 41.6A (2004), pp. 797–806. ISSN: 0748-7711. DOI: 10.1682/JRRD.2003.10.0159.
- [3] DANIEL GOLDMAN and ALEKSANDER S. POPEL. “A Computational Study of the Effect of Vasomotion on Oxygen Transport from Capillary Networks”. In: *Journal of Theoretical Biology* 209.2 (2001), pp. 189–199. ISSN: 00225193. DOI: 10.1006/jtbi.2000.2254. URL: <http://linkinghub.elsevier.com/retrieve/pii/S0022519300922549>.
- [4] Steven S. Segal. “Regulation of blood flow in the microcirculation”. In: *Microcirculation* 12.1 (2005), pp. 33–45. ISSN: 10739688. DOI: 10.1080/10739680590895028.
- [5] Can Ince. “The microcirculation is the motor of sepsis.” In: *Critical care (London, England)* 9 Suppl 4. Suppl 4 (2005), S13–9. ISSN: 1466-609X. DOI: 10.1186/cc3753. URL: <http://www.ncbi.nlm.nih.gov/pubmed/16168069%7B%5C%7D5Cnhttp://www.pubmedcentral.nih.gov/articlerender.fcgi?artid=PMC3226164>.
- [6] H. Nilsson. “Vasomotion: Mechanisms and Physiological Importance”. In: *Molecular Interventions* 3.2 (2003), pp. 79–89. ISSN: 1534-0384. DOI: 10.1124/mi.3.2.79. URL: <http://molinterv.aspetjournals.org/cgi/doi/10.1124/mi.3.2.79>.
- [7] Marc Thiriet. “Biology and Mechanics of Blood Flows - Part II: Mechanics and Medical Aspects”. In: () .
- [8] Abraham Noordergraaf. *Blood in Motion*. 2011.
- [9] Marie Dam Lauridsen et al. “Positive predictive value of International Classification of Diseases, 10th revision, diagnosis codes for cardiogenic, hypovolemic, and septic shock in the Danish National Patient Registry”. In: *BMC Med Res Methodol* 15 (215). URL: <https://www.ncbi.nlm.nih.gov/pmc/articles/PMC4373092/>.
- [10] Daniel Vincent, Jean-Louis; De Baker. “Circulatory Shock”. In: *N Engl J Med* 369.Critical Care Medicine (2013), pp. 1726–1734. URL: <http://www.nejm.org/doi/full/10.1056/NEJMra1208943>.
- [11] Ronald V. Maier. “Approach to the Patient with Shock”. In: *Harrison’s Principles of medicine* 18 (2012). URL: <http://accessmedicine.mhmedical.com/content.aspx?bookid=331%7B%5C%7Dsectionid=40727056>.
- [12] Robert H. Shmerling Ryszard M. Pluta. “Jama patient page - Sepsis”. In: 308.20 (2010), p. 7424.

Bibliography

- [13] Saowanee Kanta, Boonyang Plangklang, and Wanchai Subsingha. "World ' s largest Science , Technology & Medicine Open Access book publisher c". In: *Energy Procedia* 56.C (2014), pp. 604–609. ISSN: 9789533070865. DOI: 10.5772/711.
- [14] Simon V. Baudouin. *Sepsis: Introduction and Epidemiology*. 2008, pp. 1–2. ISBN: 9781846289385. DOI: 10.1007/978-1-84628-939-2_1.
- [15] a a Sagaidachnyi et al. "Determination of the amplitude and phase relationships between oscillations in skin temperature and photoplethysmography-measured blood flow in fingertips." In: *Physiological measurement* 35.2 (2014), pp. 153–66. ISSN: 1361-6579. DOI: 10.1088/0967-3334/35/2/153. URL: <http://www.ncbi.nlm.nih.gov/pubmed/24399251>.
- [16] A A Sagaidachnyi et al. "Thermography-based blood flow imaging in human skin of the hands and feet: a spectral filtering approach". In: *Physiological Measurement* 38.2 (2017), pp. 272–288. ISSN: 0967-3334. DOI: 10 . 1088 / 1361 - 6579 / aa4eaf. URL: <http://www.ncbi.nlm.nih.gov/pubmed/28099162%7B%5C%7D5Cnhttp://stacks.iop.org/0967-3334/38/i=2/a=272?key=crossref.169506a8780bc72b4d9d219e09a28a32>.
- [17] Wei Min Liu et al. "Reconstruction of thermographic signals to map perforator vessels in humans". In: *Quantitative InfraRed Thermography Journal* 9.2 (2012), pp. 123–133. ISSN: 21167176. DOI: 10.1080/17686733.2012.737157.
- [18] Sergey Podtaev, Matvey Morozov, and Peter Frick. "Wavelet-based correlations of skin temperature and blood flow oscillations". In: *Cardiovascular Engineering* 8.3 (2008), pp. 185–189. ISSN: 15678822. DOI: 10.1007/s10558-008-9055-y.
- [19] R Matthew Brothers et al. "Methodological assessment of skin and limb blood flows in the human forearm during thermal and baroreceptor provocations". In: *J Appl Physiol* 109 (2010), pp. 895–900. ISSN: 8750-7587. DOI: 10.1152/japplphysiol.00319.2010.â€ťSkin.
- [20] Jose Ignacio et al. *Application of Infrared Thermography in Sports Science*. 2017, pp. 49–79. ISBN: 978-3-319-47409-0. DOI: 10.1007/978-3-319-47410-6. URL: <http://link.springer.com/10.1007/978-3-319-47410-6>.
- [21] Optris. "BASIC PRINCIPLES of non-contact temperature measurement". In: (2009), pp. 1–7. URL: www.optris.com/applications?file=t1%7B%5C%7Dfiles/pdf/.../IR-Basics.pdf.
- [22] Robert Olbrycht and Boguslaw Wiecek. "New approach to thermal drift correction in microbolometer thermal cameras". In: *Quantitative InfraRed Thermography Journal* 12.2 (2015), pp. 184–195. ISSN: 21167176. DOI: 10.1080/17686733.2015.1055675. URL: <http://dx.doi.org/10.1080/17686733.2015.1055675>.
- [23] L. Schacher, D.C. Adolphe, and J.-Y. Drean. "Comparison between thermal insulation and thermal properties of classical and microfibres polyester fabrics". In: *International Journal of Clothing Science and Technology* 12.2 (2000), pp. 84–95. URL: <https://doi.org/10.1108/09556220010371711>.

Bibliography

- [24] J. Grant Mouser et al. “A tale of three cuffs: the hemodynamics of blood flow restriction”. In: *European Journal of Applied Physiology* 117.7 (2017), pp. 1493–1499. ISSN: 14396319. DOI: 10.1007/s00421-017-3644-7.
- [25] Martin H. Weik. *Nyquist sampling rate*. 2000. DOI: 10.1007/1-4020-0613-6_12653. URL: https://link.springer.com/referenceworkentry/10.1007/1-4020-0613-6%7B%5C_%7D12653.
- [26] Cintia Bertacchi Uvo. “Fourier and Wavelets Transforms”. In: (1995), pp. 1–19.
- [27] Luís Aguiar-Conraria and Maria Joana Soares. “The Continuous Wavelet Transform: A Primer”. In: *NIPE-Universidade do Minho* (2011), pp. 1–43. URL: http://www.economics-ejournal.org/economics/journalarticles/2011-16/references/@@export%7B%5C%7D5Cnhttp://www.eeg.uminho.pt/economia/nipe%7B%5C%7D0A*.
- [28] MathWorks. *Continuous 1-D wavelet transform*. 2017. URL: https://se.mathworks.com/help/wavelet/ref/cwt.html?searchHighlight=cwt%7B%5C&%7Ds%7B%5C_%7Dtid=doc%7B%5C_%7Dsrchtitle (visited on 01/01/2017).
- [29] M. L. Iabichella, E. Melillo, and G. Mosti. “A Review of Microvascular Measurements in Wound Healing”. In: *The International Journal of Lower Extremity Wounds* 5.3 (2006), pp. 181–199. ISSN: 1534-7346. DOI: 10.1177/1534734606292492. URL: <http://journals.sagepub.com/doi/10.1177/1534734606292492>.
- [30] Anders Eriksen, Dominik Osinski, and Dag Roar Hjelme. “Evaluation of thermal imaging system and thermal radiation detector for real-time condition monitoring of high power frequency converters”. In: *Advances in Manufacturing* 2.1 (2014), pp. 88–94. ISSN: 21953597. DOI: 10.1007/s40436-014-0066-1.
- [31] Alejandro Wolf, Jorge E. Pezoa, and Miguel Figueroa. “Modeling and compensating temperature-dependent non-uniformity noise in IR microbolometer cameras”. In: *Sensors (Switzerland)* 16.7 (2016), pp. 1–13. ISSN: 14248220. DOI: 10.3390/s16071121.
- [32] T. Hida and Si Si. “Lectures on White Noise Functionals”. In: (2014), pp. 13–62.
- [33] Jerrold H. Zar. *Biostatistical Analysis*. Internatio. Pearson, 2014, p. 751. ISBN: 1-292-02404-6.
- [34] Usman Mohammed Akeyede Imam and Moses Abanyam. “On Consistency and Limitation of paired t-test, Sign and Wilcoxon Sign Rank Test”. In: *IOSR Journal of Mathematics (IOSR-JM)* 10.1 (2014), pp. 01–06. URL: <http://www.iosrjournals.org/iosr-jm/papers/Vol10-issue1/Version-4/A010140106.pdf>.
- [35] Andrey Sagaidachnyi et al. “Restoration of finger blood flow oscillations by means of thermal imaging”. In: *11th International Conference on Quantitative InfraRed Thermography, Naples Italy* (2012), pp. 1–8.

A | Protocol

Experimental Protocol

Experiment

Study of temperature oscillations in the peripheral circulation with infrared thermography

Formalities

Date:	17.10.2017 and 18.10.2017
Place:	Regionshospital Nordjylland in Hjørring
Conducted by:	Toby Waterstone, Christian Mortensen, Annabel Bantle, Andrei Ciubotariu

Background

Aim:	The aim of the experiment is to measure vasomotion in the hand in two conditions
Type of study:	Quantitative research
Subjects:	<p>Number of subjects: 4</p> <p>Inclusion criteria:</p> <ul style="list-style-type: none">• Subjects should have at least one hand to perform the measure on• The cuff should be able to fit the arm circumference• The subject should be able to sit still for a greater extend of time• Health conditions that sets the subject in risk of injury when conducting the experiment like high blood pressure. <p>Exclusion criteria:</p> <ul style="list-style-type: none">• Age under 18 years old• Age over 60 years old• Obesity to a greater extend• Diseases that triggers tremors

Test Requirements

Materials:	Xenics Gobi 640 17µm GigE Infrared camera with power cord, Tripod, Cuff, Chair, Computer with recording software and power
------------	--

Experimental Protocol

	cord, Vacuum pillow, Vacuum pump, Stopwatch, Ethernet cable, Computer.
Setup:	
Preparation:	<ol style="list-style-type: none">1. The camera has to warm up for 15 min.2. During this laptop, software and all cable connections should be set in operational readiness.
Procedure:	<ol style="list-style-type: none">1. Systolic pressure is measured and mean is calculated2. Pressure to be used in cuff is calculated3. The cuff is affixed at the subjects dominant arm without tighten it.4. The subject can take place in the chair.5. The hand is put on the vacuum pillow.6. The vacuum pump is attached to the pillow.7. The camera needs to be positioned 37.5 cm over the hand with the focus adjusted.8. If the camera is stable, the first measurement can be started for exact 20 min.9. Save file as subject_number of subject.10. Tighten the cuff on the arm of the subject with XXX, without moving the subjects hand.11. The second measurement can be started for exact 20 min.12. Maintain same pressure for 20 min.13. Save file as subject_number of subject_cuff

Appendix A. Protocol

Table A.1: Table of blood pressure.

Subject number	1. systolic pressure	2. systolic pressure	3. systolic pressure	Mean pressure	30 % of TOP
1	141 mmHg	138 mmHg	137 mmHg	138.6 mmHg	54.08 mmHg
2	102 mmHg	102 mmHg	102 mmHg	102 mmHg	39.78 mmHg
3	155 mmHg	147 mmHg	146 mmHg	149.3 mmHg	58.24 mmHg
4	138 mmHg	145 mmHg	135 mmHg	139.3 mmHg	54.34 mmHg

B | Evaluation table

ROI	S1_U	S1_C	S2_U	S2_C	S3_U	S3_C	S4_U	S4_C
1	✗	✗	✓	✗	✗	✓	●	✗
2	✓	✓	✓	✓	✗	✓	✓	✓
3	✓	✓	✓	✓	✗	✓	✓	✓
4	✓	✓	✓	✓	✗	●	✓	✓
5	✗	✗	✓	✗	✗	✓	✓	✗
6	●	●	✓	✓	✗	✓	✓	✗
7	✓	✓	✓	✓	✗	✓	✓	✓
8	✓	✓	✓	✓	✓	✓	●	✓
9	✓	✓	✓	✓	●	✓	✓	✓
10	✓	✓	✓	✓	✓	✓	✓	✓
11	✗	✗	✓	✗	✗	✓	✓	✗
12	✓	✓	✓	✓	✗	✓	✓	●
13	✓	✓	✓	✓	✗	✓	✓	✓
14	✓	✓	✓	✓	✓	✓	✓	✓
15	✓	✓	✓	✓	✗	●	✓	✓
16	✓	✓	✓	✓	✗	●	✓	✓
17	●	✗	✓	✗	✗	✓	✓	✗
18	✓	✓	✓	✗	✗	✓	✓	●
19	✓	✓	✓	✓	✗	✓	✓	✓
20	✓	✓	✓	✓	✓	✓	✓	✓
21	✓	✓	✓	✓	✓	✓	✓	✓
22	✓	✓	✓	✓	✓	✓	✓	✓
23	●	✗	✓	✗	✗	✓	✓	✗
24	●	●	✓	✗	✗	✓	✓	✗
25	●	✓	✓	✓	✗	✓	✓	✓
26	✓	✓	✓	✓	●	✓	●	✓
27	✓	✓	✓	✓	✗	✓	●	✓
28	✓	✓	✓	✓	✗	✓	✓	✓

Legend

✓	ROI in this recording useful
●	ROI in this recording maybe useful
✗	ROI in this recording not useful
■	ROI used for data analysis
	ROI is improper for data analysis
■■	ROI cannot be used for data analysis